International Journal of Thermophysics (2020) 41:157
https://doi.org/10.1007/s10765-020-02737-1

Nanofluids in Solar Thermal Collectors: Review and Limitations

Ifeoluwa Wole-osho[1] · Eric C. Okonkwo[1,2] · Serkan Abbasoglu[1] · Doga Kavaz[3]

Received: 13 June 2020 / Accepted: 10 September 2020 / Published online: 23 September 2020

Abstract

Solar thermal collectors are systems that allow for the use of solar energy in thermal applications. These collectors utilize a heat transfer fluid to transport absorbed solar radiation to applications where they are needed. Scientists in a bid to improve the conversion efficiency of solar collectors have suggested different collector designs and improved collector materials. Over the last 25 years, the study of nanofluids and their applications have revolutionized material science, and nanotechnology has found applications in improving solar collector materials. This article reviews the impact of different nanomaterials on the efficiency of solar collectors. The study also outlines the limitations of applying nanofluids and discusses the long-term challenges of their application to solar collectors. Nanofluids have the potential to improve the overall efficiency of most solar collectors, however, the full potential of nanofluids in heat transfer applications cannot be completely achieved until some of the questions regarding hysteresis, stability, and the overall predictability of nanofluids are answered.

Keywords Compound parabolic collector · Evacuated tube collector · Flat plate collector · Nanofluid · Parabolic trough collector · Solar collector

Abbreviations

ASHRAE	American Society of Heating, Refrigeration and Air Condition Engineers
ASTM	American Society for Testing and Materials
Conc	Concentration
CPC	Compound parabolic collector

✉ Eric C. Okonkwo
eokonkwo@hbku.edu.qa

[1] Department of Energy Systems Engineering, Cyprus International University, Nicosia, North Cyprus, Turkey

[2] Division of Sustainable Development, College of Science and Engineering, Hamad Bin Khalifa University, Qatar Foundation, Education City, Doha, Qatar

[3] Department of Bioengineering, Cyprus International University, Nicosia, North Cyprus, Turkey

ETC	Evacuated tube collector
FPC	Flat plate collector
HTF	Heat transfer fluid
PTC	Parabolic through collector:
SEM	Scanning electron microscope
STC	Solar thermal collectors
XRD	X-ray diffraction
Vol	Volume

List of Symbols

A	Area (m^2)
A_l	Aperture of area (m^2)
A_t	Area of surface (m^2)
c	Speed of light
Cp	Specific heat capacity ($kJ{\cdot}kg^{-1}{\cdot}K$)
C_r	Concentration ratio
d	Distance
D	Diameter (m)
D_i	Inlet diameter (m)
E	Energy (J)
E_g	Stefan–Boltzmann constant
f	Wavelength
f	Friction factor
F'	Collector efficiency
F_R	Heat removal factor
g	Acceleration due to gravity
G	Direct normal irradiance ($W{\cdot}m^{-2}$)
I	Current (A)
h	Heat transfer coefficient ($W{\cdot}m^{-2}{\cdot}K$)
Hz	Hertz
k	Thermal conductivity ($W{\cdot}m^{-1}{\cdot}K$)
L	Length (m)
m	Mass flow rate ($kg{\cdot}min^{-1}$)
m	Mass
N	Number of glass cover
Nu	Nusselt number
P	Pressure
Pr	Prandtl number
Q_u	Useful energy
Q	Heat flux (W)
Re	Reynolds number
T	Temperature (K)
U_L	Heat loss coefficient ($W{\cdot}m^{-2}{\cdot}K$)
v	Velocity (m·s)
V_f	Volumetric flow rate ($L{\cdot}min^{-1}$)
w	Tape width

W	Tube spacing
x	Direction (mm

Greek Symbols

ΔP	Pressure drop (kPa)
ΔT	Difference between inlet and ambient temperatures (K)
η	Efficiency
θ	Incident angle
μ	Dynamic viscosity (Pa s)
ρ	Density (m^3)
φ	Volume concentration
α	Absorber absorbance, respectively
β	Slope of collector
γ	Arbitrary wedge
γ	Intercept factor
ε	Emissivity
σ	Stefan–Boltzmann constant
τ	Cover transmittance

Subscript/Superscript

a	Ambient
bf	Base fluid
c	Collector
ci	Inner cover
co	Outer cover
cs	Cross section
eff	Effective
ex	Exergetic
f	Fluid
fm	Mean fluid
g	Glass cover
gi	Inner glass cover
h	Hydraulic
in	Inlet
k	Component
loss	Loss
nf	Nanofluids
nnp	Number of nanoparticles
np	Nanoparticles
o	Outlet
opt	Optical
p	Plate
r	Receiver
ri	Inner receiver
ro	Outer receiver
s	Solar

sun	Sun
th	Thermal
u	Useful

1 Introduction

As energy demands continue to increase exponentially, environmental concerns related to fossil fuel consumption are on the rise. The efficient utilization of various forms of renewable energy has been an objective of many energy studies. Solar energy is currently the most consumed form of renewable energy [1]. Solar energy can be harnessed for heating and cooling buildings [2], domestic water heating [3], water desalination [4], and many industrial applications. Various inventions have enabled more efficient utilization [5] and storage of solar energy [6]. Solar collectors are the devices used to absorb the energy from the sun and repurpose it for direct or indirect human consumption. Even though the basic principles of these solar devices have been available since the 1700s. Our constantly improving understanding of conduction, convection, radiation, photoelectric effect, and the material sciences have enabled us to build more efficient solar collectors. Improvement in these devices has reduced dependence on conventional fossil fuels for energy. Solar collectors are wave absorbance mediums that convert solar radiation to thermal or electrical energy [7]. Solar photovoltaic (PV) collectors convert solar radiation to electrical energy, solar thermal collectors (STC) convert solar irradiation to thermal energy while solar photovoltaic thermal collectors (PTC) converts incident solar irradiation to both thermal and electrical energy.

Modern designs, especially in solar thermal collector technology, have increased the share of energy consumption obtained from solar energy. The solar thermal collector is a heat exchanger where a selective material absorbs radiation from the sun; this absorbed thermal energy is then transferred to a working fluid (air, water, nanofluid, or oil) for use in other applications. Even though the thermal efficiency of these collectors has generally improved with time, further improvement in the thermal efficiency of these collector systems must continue until they reach the maximum attainable system efficiency. Nanofluids presents a significant opportunity to improve the thermal efficiency of these heat collector systems. Since Choi and Eastman [8] published the study that showed that the thermal conductivity property of base fluids can be improved by nanoparticle dispersions. Several researchers have tried to apply these nanofluids in different heat transfer systems with their experiments having various degrees of success [9–11]. This study intends to track the progress that has been made in the application of nanofluids in various solar thermal collectors. It investigates recently published works to determine the potential limitations that exist in the application of nanofluids in solar collectors. First, the basic physical principles of solar collectors' systems are discussed. Then, the study discusses the nanofluid synthesis, stability, and thermophysical properties. Also, a comprehensive review of the application of nanofluids in solar collector systems is presented, and finally, the current limitations to their application in solar collectors are discussed.

2 Solar Collector Systems

As solar collector designs have improved two main classifications for solar thermal collectors have emerged. These are non-concentrating collectors and concentrating collectors [12]. Figure 1 shows the various classification of solar collectors.

The main difference between the non-concentrating STC and the concentrating solar thermal collectors is the difference in the ratio between the collector area and the absorbing region. Non-concentrating STC has a collector surface area, which is equal to the absorber area. In contrast to concentrating solar thermal collectors, the collector area is larger than the absorbing region [13]. Evacuated tube collectors (ETC) and flat plate collectors (FPC) and are the main commercial non-concentrating collectors available. The working fluid temperatures can range between 303 and 423 K depending on the collector system [14]. For concentrating solar collectors, mirrors, reflectors, or solar trackers are used to focus solar radiation from the collector area to the absorbing area. Concentrating collectors have working fluids that operate at much higher temperatures than non-concentrating collectors. Table 1 presents the concentration ratios and upper-temperature limits of these collectors.

The remainder of this section will present the working principles of the various collectors investigated in this study along with the recent advances by researchers to improve the thermal efficiency of these collectors.

2.1 Flat Plate Collectors (FPC)

Flat plate solar collectors (FPC) are the most widely used solar thermal collectors [15]. The collector, first designed by Hottel [16], is primarily composed of an absorber surface, a transparent cover, risers, and insulation. The absorber surface is

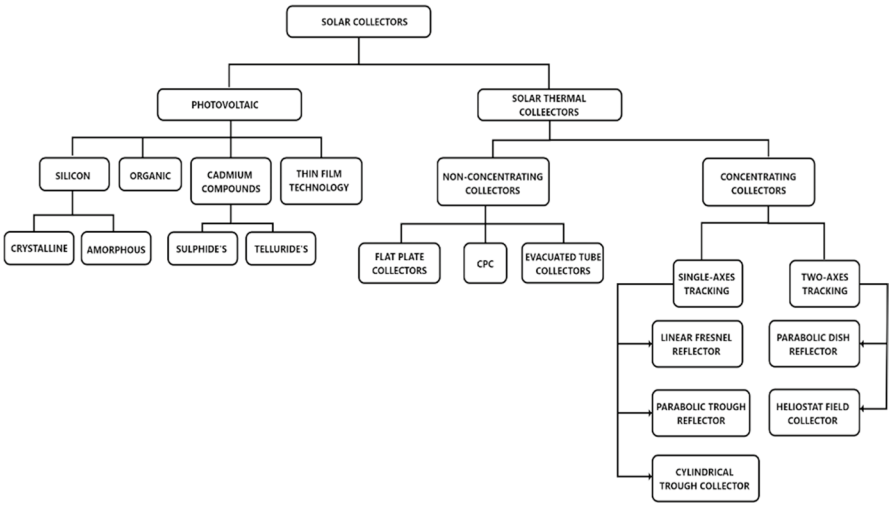

Fig. 1 Classification of solar collectors

Table 1 Solar thermal collectors operating temperatures and concentration ratios

Collectors	Concentration ratio	Maximum operating temperature (°C)
Flat plate	1	80
Evacuated tube	1	150
Compound parabolic	1–5	200
Parabolic trough	10–80	400–500
Linear Fresnel	10–400	450
Solar dish	~1000	600

a black surface intended to collect as much thermal energy as possible [12]. Thermal energy received on the absorber plate is transferred to the working fluid (air, water, etc.) in the risers (pipes) by convective heat transfer. The schematic of the flat plate collector is shown in Fig. 2.

Even though FPCs are the most used collectors, they are the least efficient of all STC. The thermal efficiency of a flat plate solar collector is simply the ratio of the useful energy (Q_u) to the total incident solar radiation [17]. Several investigations have been done to improve the thermal efficiency of flat plate collectors. Mansour [18] introduced the use of novel mini channels in the FPC. This novel design improved the heat removal factor in the collector. The study observed deviations as high as 10%, between the thermal efficiency results from theoretical models and results from experiments. Deng et al. [19] also designed a novel flat plate solar collector with a micro-channel heat pipe array; the experiment showed that the maximum instantaneous efficiency of the collector was 80%.

Improving the flat plate collector's efficiency by enhancing the absorber material coating is another important research area. Föste et al. [20] presented a thermochromic absorber coating; this absorber material has a unique behavior, as they can change their emissivity by a factor of 0.35 depending on temperature. The overall system performance was increased from 1.5% to 4.5% by using this thermochromic absorber coating compared to conventional absorber coating. Jyothi et al. [21] designed a novel 5-layered nanostructure of TiAlC/TiAlCN/TiAlSiCN/TiAlSiCO/TiAlSiO tandem absorber. This absorber-reflector tandem has TiAlC, TiAlCN, and TiAlSiCN as the absorbing layer; with TiAlSiCO and TiAlSiO act as semi-transparent and anti-reflecting layers. In application, the absorption material is stable to up to 598 K in the air for 400 h and 923 K in vacuum for 100 h. Unfortunately, when operating under higher temperatures tandem absorbers tend to degrade because of the relatively unstable microstructure [22].

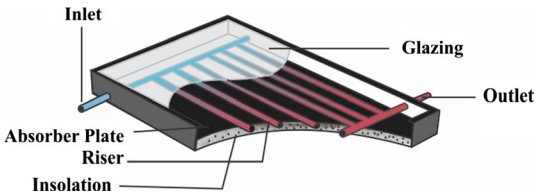

Fig. 2 Diagram of a flat plate solar collector (FPC)

The glazing on the top of the flat plate collector primarily functions to reduce convective and radiative losses from the absorber, transmit the incident solar radiation into the absorber plate, and protect the system from environmental damage. Effective glazings have low reflection and absorption properties while having high transmission properties [23]. Glazing materials are doped with transparent conductive oxides (TCO) like aluminum-doped zinc oxide and tin-doped indium oxide [24] to improve the glazing transmittance performance.

Recently, a growing number of studies have focused on enhancing the overall thermal efficiency of collectors by improving the properties of their heat transfer fluids (HTF). These working fluids have been improved by replacing the conventional HTF with a mixture of glycol, propylene, and water. These mixtures have been proven to slightly improve the thermal performance of the collectors [25], however, the potentials of nanofluids in improving the thermal efficiency of solar thermal collectors are enormous.

2.1.1 Thermal Analysis of Flat Plate Collectors

The useful energy (Q_u) of an FPC with a collector area A_t can be defined as [17]:

$$Q_u = I_t.A_t.(\tau\alpha)_{eff} - U_l, \tag{1}$$

where I_t is solar radiation on the absorber surface, A_t is collector surface area, $(\tau\alpha)_{\text{eff}}$ is the product of the cover transmittance, and absorber surface absorptance, and U_l is the collector's heat loss to the surroundings.

The energy efficiency (η) of the collector is the ratio of useful energy (Q_u) to the total incident radiation on the absorber area [26]:

$$\eta = \frac{Q_u}{I_t.A_t}. \tag{2}$$

In experiments, useful energy is calculated with Eq. 3 [17]:

$$Q_u = F_R.A_t\left[I_t(\tau\alpha)_{eff} - U_l\left(T_i - T_a\right)\right], \tag{3}$$

where F_R heat removal factor, T_i is the inlet temperature, and T_a is the ambient temperature.

2.2 Evacuated Tube Collectors

Evacuated tube collectors (ETC) often display improved efficiencies over varying operating conditions when compared to the flat plate collector [27–29]. ETC has a vacuum that exists between the outer glass tube and the absorber, imitating the thermo-flask effect, as the vacuum between both mediums acts as the insulation. The outer glass reduces radiative losses from the collector; the glass allows shortwave radiation from the sun and also preventing long-waves from being lost through the glass tube [30].

As seen in Fig. 3, a heat pipe is attached to the absorber plate, contained within the heat pipe is a working fluid that evaporates and condenses, as heat transfer occurs between the heat pipe condenser and the heat transfer fluid. The fluid with the heat pipe is heated by the collector material until evaporation occurs. As the evaporate diffuses to the top, it losses to cooler conditions within the manifold causing the evaporate to condense further losing latent heat. The vacuum insulation in the ETC makes them uniquely able to reduce losses to the environment; the internal temperature within the tube may be as high as 423 K while the external surface remains at ambient temperature. There are two types of ETC, namely; heat pipe-ETC (HP-ETC) tube and direct flow ETC (U-Tube-ETC, single-walled glass ETC).

2.2.1 Thermal Analysis of Evacuated Tube Collectors

Two methods can be used to determine the efficiency parameters of ETC: The quasi-dynamic test method and the steady-state test method. The steady-state method requires that all boundary conditions are set as constant, while transient or quasi-dynamic state boundary conditions may vary with time [31].

The heat rate gained by the fluid in ETC is then given by [32]

$$Q_u = \dot{m}.C_p.\Delta T, \tag{4}$$

where $\dot{m}$, C_p, and ΔT represents the mass flow rate of the fluids, the specific heat capacity, and the difference between the inlet and outlet temperatures.

The thermal efficiency "η" of the ETC is also the ratio of the useful energy (Q_u) to the total incident solar radiation "G", on the collector area (A_t) [32]:

$$\eta = \frac{Q_u}{G.A_t}. \tag{5}$$

The useful energy from the system can be further described as a function of the heat removal factor F_R of the system [32]:

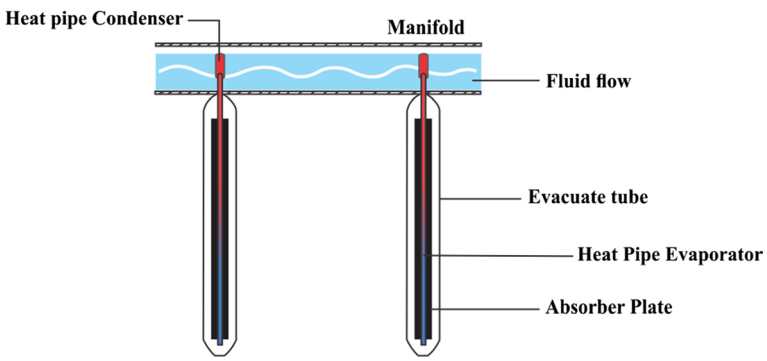

Fig. 3 Diagram of a heat pipe evacuated tube collector (ETC)

$$Q = A_t F_R \left[G - U_L \left(T_m - T_a \right) \right], \tag{6}$$

where U_l is the overall heat loss coefficient.

2.3 Compound Parabolic Collectors (CPC)

The compound parabolic collector was first designed by Winston [33]. CPC uses parabolic optics to concentrate incident solar radiation over an aperture of area A_L and concentrate it on a smaller absorber area A_s. Like the flat plate and evacuated tube collectors, the CPC is static when collecting diffuse solar radiation. There are four kinds of CPC, namely: flat one-sided absorbers; the flat two-sided absorbers, wedge-like absorbers, and tubular absorbers. The concentration ratio C_R is the ratio of the aperture area to the absorber area [34]:

$$C_R = \frac{A_L}{A_s}. \tag{7}$$

As seen in Fig. 4, a flat one-sided absorber contains a parabolic collector surface and a flat blacken absorber.

The area of the absorber is the product of the length of the tube (L), and the breath of the flat absorber (l_p) [34].

$$A_s = l_p.L. \tag{8}$$

The concentration ratio of CPC is given in Eq. 9 [34]:

$$C_r = \frac{1}{\sin(\frac{1}{2}\theta_a)}, \tag{9}$$

where θ_a is the acceptance angle. From Fig. 4b, the absorber plate of the flat bifacial CPC is vertically place within the parabolic reflector, doubling the area of absorption compared to the flat one-sided CPC [36]. From Fig. 4c, the wedge absorber is within the truncated parabolic reflector surfaces. A vital point to make is that the flat bifacial CPC and the flat one-side CPC can both be described as forms of the wedge absorbers.

If we assume an arbitrary wedge separation angle (γ); for the flat bifacial absorbers $\gamma = 90^0$, and for the flat one-side absorber $\gamma = O^0$. The wedge-shaped absorbers CPC $\gamma = \delta_i$. According to Baum and Gordon [37], the wedge-shaped absorbers CPC saves on the reflector area compared to both flat bifacial CPC and flat one-side CPC.

The cylindrical shape of the absorber plate in tubular CPC creates non-uniform irradiation around the absorber; this leads to hotspots (high intensity). The lack of uniformity in received irradiation reduces the working efficiency of the tubular absorber CPC. The area of absorption in tubular CPC is equal to the surface area of the cylinder [38]:

$$A_s = 2\pi rl, \tag{10}$$

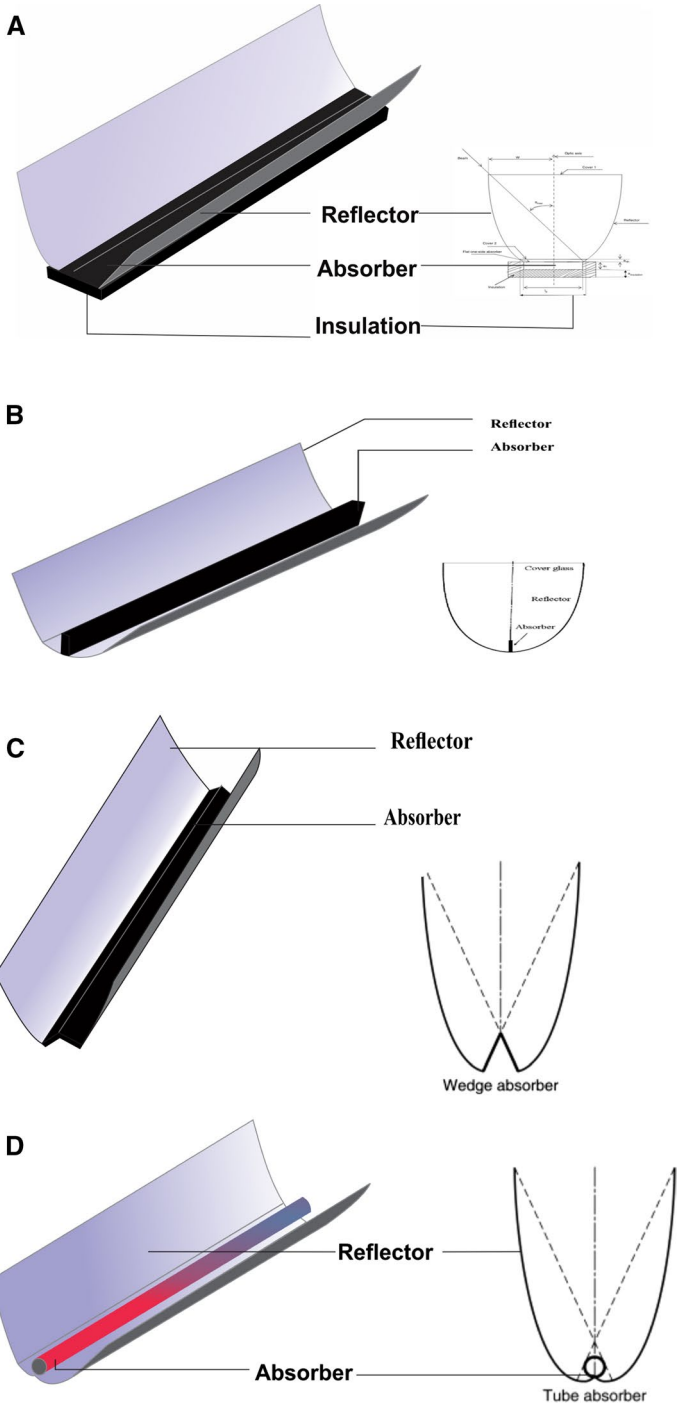

Fig. 4 Cross section of CPC (a) flat one-sided absorber [35], (b) flat bifacial absorbers, (c) wedge-shaped absorber, (d) tubular absorber

where r is the radius of the tubular absorber and l is the length of the absorber.

2.4 Parabolic Trough Collector (PTC)

The PTC remains the most commercially mature solar concentrating collector to date [39, 40]. PTCs are cost-effective and have the highest deploy-ability globally of all concentrating solar collectors. It is a line concentrating collector and collects solar radiation incident on it using a parabola-shaped reflective surface. A receiver tube placed at the focal length of the parabolic collector collects incident solar radiation. The receiver transfers the thermal energy into the heat transfer fluid passing through it by way of convection. The useful thermal energy gained is used for various applications ranging from electricity production, absorption cooling, industrial process, desalination, etc. The operating temperature of the PTC ranges from 50 °C to 400 °C and the working fluids used include gases, water, and synthetic thermal oils. Figure 5 shows a diagram of the parabolic trough collector.

The thermal efficiency of the system can range from 65% to 75%. The use of nanoscale particles in the heat transfer fluid has gained wide research attention as both theoretical and experimental studies have been carried out to ascertain the benefits of nanofluids in the parabolic trough collector (PTC). One of the benefits of the use of nanofluids in the PTC, just like in the non-concentrating collectors is the improved thermal conductivity of the working fluids. The increased thermal conductivity improves the rate of heat transfer from the absorber tube walls to the working fluids and hence leads to enhanced collector efficiency.

2.4.1 Thermal Model of Parabolic Trough Collector

Solar energy incident on the collector can be calculated with:

$$\dot{Q}_s = A_s \bullet G. \tag{11}$$

The useful energy obtained from the system is presented as [41]:

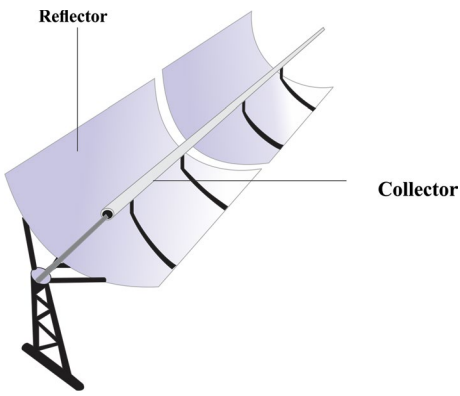

Fig. 5 Schematic diagram of a parabolic trough collector

$$Q_u = \dot{m} \cdot C_p \cdot \left(T_{out} - T_{in}\right). \tag{12}$$

The thermal efficiency of the trough collector can thus be calculated by applying Eq. 13 [42]:

$$\eta_{th} = \frac{Q_u}{Q_s} \tag{13}$$

where Q_u represents the useful energy obtainable by the collector and Q_s represent the energy from the sun.

There are various losses associated with the collector and they can all be expressed by the heat loss coefficient (U_L). The derivation of this parameter is defined by the various thermal losses (Q_{loss}) associated with the heat transfer in the collector as well as the area of the receiver (A_{ro}), and the temperature of the receiver (T_r) [39]:

$$U_L = \frac{Q_{loss}}{A_{ro}(T_r - T_{amb})}, \tag{14}$$

$$Q_{loss} = \frac{2\pi k_{eff} L}{\ln(D_{co}/D_{ci})}\left(T_r + T_{ci}\right) + \frac{\pi \cdot D_{ro} \bullet L \bullet \sigma \bullet (T_{ro}^4 - T_{gi}^4)}{\frac{1}{\varepsilon_r} + \frac{1-\varepsilon_g}{\varepsilon_g} \bullet \frac{D_{ro}}{D_{ci}}}, \tag{15}$$

where k_{eff} represents the effective thermal conductivity, D_{co} represents the outer diameter of the cover, D_{ci} represents the inner diameter of the cover and T_{ci} inner temperature of the glass cover. The value of the effective thermal conductivity is suppressed to zero at low pressures. The thermal losses include the convective and radiative losses from the surface of the receiver tube and the conductive losses through the support structure [39]:

$$Q_{loss} = \underbrace{\pi D_{co} L h_w (T_{CO} - T_a)}_{convective\ heat\ loss} + \underbrace{\varepsilon_{co} \pi D_{co} L \sigma (T_{co}^4 - T_{sky}^4)}_{radiative\ heat\ loss}, \tag{16}$$

where T_r represents the temperature of the receiver, h_w is the heat convection coefficient of the wind [43]:

$$h_w = u_w^{0.58} \bullet D_{co}^{-0.42}, \tag{17}$$

$$T_{sky} = 0.0552 T_a^{1.5}. \tag{18}$$

3 Nanofluids and Their Thermal Properties

Nanofluids are a new class of fluids that contain nanometer-sized particles suspended within a base fluid [44, 45]. The volume of nanoparticles within the base fluid is measured by the percentage volume fraction or volume concentration. The volume concentration of nanofluids is given by Eq. 19:

$$\varphi = \%Volumetric\ concentration = \frac{\frac{W_{np}}{\rho_{np}}}{\left[\frac{W_{np}}{\rho_{np}}\right] + V_b} \times 100, \tag{19}$$

where ρ_{np}, V_b,W_{np}, and nnp represent, nanoparticle density, base fluid volume, nanoparticle weight, and the number of types of nanoparticles, respectively.

Since Maxwell published the theoretical possibility of particle dispersions in improving the thermal conductivity of fluids over a century ago [46]. There have been several experimental and theoretical research into metallic particles suspension in fluids and the applications of these fluids in heat transfer. The initial research undertaken by Maxwell focused on microparticle suspension. The problems that exist with microparticle suspension; is that metallic microparticles were not stable, as the particles quickly descended to the base and the fluid. Nanoparticles are at least 1000 times smaller in size than microparticles and can be dispersed uniformly and therefore have significantly better thermal performance [47].

3.1 Nanofluid Synthesis Techniques and Stability

There are three main techniques used to prepare nanofluids, namely, the one-step chemical method, the one-step physical method, and the two-step method.

In the two-step method of nanofluid preparation, the nanoparticles are synthesized and then are dispersed into the base fluids [48]. Nanoparticles can be synthesized by precipitation [49], chemical reduction [50], or crystallization [51]. The two-step method is the most common method in nanofluid preparation because it allows for the easy control of the volume fractions of the nanoparticle in the mixture. Just within the past year, several researchers have applied the two-step process in developing nanofluid material. Asadi et al. [52], Almanassra et al. [53], and Chen et al. [54] all applied the two-step process in synthesizing MWCNTs–water nanofluids. This method has also been used for metal oxide nanofluids like CuO water nanofluid [55], Fe_2O_3 water nanofluid [56], SiO_2 glycerol–water nanofluid [57] and have also been used in the synthesis of hybrid nanofluids [58–60].

The one-step physical method heats electrodes by arc sparking and condenses it into the liquid. The one-step method allows for better nanofluid stability and thermal conductivity properties to be controlled. However, it is difficult to produce a large volume of nanofluids [61]. One-step chemical method is an adaptation of the Schlenk technique [62], like in One-step physical method nanoparticles are synthesized within the fluid. This technique allows for the control of nanoparticle size and nanofluids prepared with this technique are most stable. However, synthesizing large

volumes of nanofluids with this method is very challenging [63]. Huang et al. [64] applied the two-step method using Field's alloy nanoparticles dispersed in polyalphaolefin (PAO), also a similar method of synthesis was applied in both Du et al. [65]. and Li et al. [66] research. It is vital to note that the pH of the nanofluid is an important parameter that directly affects the long-term stability of the nanofluid. As observed by Wole-Osho et al. [67], Okonkwo et al. [48], and Wang et al. [68] both conventional and hybrid nanofluids tend to be more stable as they become either more acidic or more alkaline. The overall stability of nanofluids is not just dependent on fluid pH but also on the nanofluid material, the synthesis technique, and the sonification time [45]. As nanofluid becomes more unstable, the more precipitates are observed within the fluid. Therefore, the stability of nanofluids is often measured by physical observation of the nanofluid. However, it is more accurate to measure the surface electrostatic repulsion force contained within the nanofluid zeta potential for a more accurate guide to the fluid's stability [48, 67, 68]. As seen in multiple studies, the stability of the nanofluids has a large range. While CuO water nanofluid can be stable for as long as one (1) year as observed by Albert et al. [69], in some other nanofluids stability is less twelve (12) hours [64, 70]. The difference in how long nanofluids are stable is likely because stability is a unique property of the synthesized fluid. Therefore even the slightest changes in fluid configuration and synthesis procedure can produce different outcomes in the stability of the fluid.

Several properties affect the rheology and thermal performance of nanofluids; these properties include density (ρ), heat capacity (C_p), thermal conductivity (k), viscosity (μ), volume concentration (ϕ), shear rate range, particle size, particle shape, etc.[45, 71]. Nanofluids are classified into hybrid nanofluids and conventional nanofluids [72]. Hybrid nanofluids have more than one nanoparticle type within the base fluid while conventional nanofluids have only one nanoparticle type within the base fluid. Often conventional nanofluids do not possess all the positive applicative properties. Some single-particle nanofluid may have favorable thermal properties and lack favorable rheological characteristics. To improve on this challenge, hybrid nanofluids are synthesized. A combination of nanoparticles with the ability to trade-off respective strengths can improve the application properties of nanofluids [73].

3.2 Density of Nanofluid

The density of a two-phase fluid is conventionally accepted to be the sum of the product of density and volume concentration for both the nanoparticle and the base fluid. The conventional formula to calculate nanofluid density is given as [74]:

$$\rho_{nf} = \rho_{np}\varphi + \rho_{bf}(1 - \varphi), \tag{20}$$

where "ρ_{nf}", "ρ_{np}", "φ" and ρ_{bf} represent the nanofluid density, the nanoparticle density, is the volume concentration, and the base fluid density [74].

3.3 Nanofluid Specific Heat Capacity (C_p)

The specific heat capacity of the nanofluids directly affects the heat recovery property of the fluid. Accurately predicting the specific heat performance of nanofluids, increases their application potentials. Therefore, numerous models have been proposed to determine the specific heat capacity of nanofluids.

As seen in Eq. 21, the specific heat of a water-based conventional nanofluid was calculated using mixture theory [74]. The model proposes that the specific heat of a nanofluid is dependent on the nanoparticle volume concentration, the specific heat of both the base fluid and the nanoparticle. However, the mixture theory model for predicting specific heat deviates significantly from the experimental data [75]:

$$C_{nf} = C_{np}\varphi + C_{bf}(1-\varphi), \tag{21}$$

where C_{bf} is the specific heat of the base fluid, C_{np} is the specific heat of the nanoparticle and φ represents volume concentration [74]

The thermal equilibrium model is another model used to predict the specific heat of nanofluids. As seen in Eq. 22 [76], the thermal equilibrium model adds nanoparticle and base-fluid densities to the variables affecting nanofluid specific heat. The thermal equilibrium model performed better than the mixture theory model, even though significant deviations still exist between the model results and experimental results [77]:

$$\rho_{nf}C_{nf} = \rho_{np}C_{np}\varphi + C_{bf}\rho_{bf}(1-\varphi), \tag{22}$$

where "C_{bf}" is the specific heat of the base fluid [76].

In this decade, other models have been proposed to predict the specific heat of nanofluids. Wang et al. [78] proposed Eq. 23, Shin, and Banerjee [79] proposed Eq. 24 using thermal equilibrium models, and Kumaresan and Velraj [80] proposed Eq. 25 for predicting specific heat:

$$C_{nf} = \left[\rho_{np}C_{np}\varphi + C_{bf}\rho_{bf}(1-\varphi)\right]/[\varphi_{bf}\rho_{bf} + (1-\varphi)\rho_{np},] \tag{23}$$

$$C_{p,t} = (\varphi\varphi_{np}C_{np} + \varphi_{bf}\rho_{bf}C_{bf})/\left(\varphi_{np}\rho_{np} + \varphi_{nf}\rho_{nf}\right), \tag{24}$$

$$C_{nf} = [\rho_{np}C_{np}\varphi + C_{bf}\rho_{bf}(1-\varphi)]/\left[\varphi\rho_{np} + (1-\varphi)\rho_{bf}\right]. \tag{25}$$

None of the proposed numerical equations accurately and consistently predicts the specific heat of nanofluids over a large range of volume concentrations. Research has found that regression correlation equations are more accurate than classical models for specific heat prediction. Vajjha and Das [81] proposed a correlation equation for the specific heat of three nanofluids. The results from the correlation equation were within an average error of about 2.7% to experimental results. Most recently, studies have focused on the use of artificial intelligence to predict this fluid property. Alade et al. [82] developed a support vector regression (SVR) model optimized with

a Bayesian algorithm (BSVR) to predict the specific heat of a glycol-based conventional nanofluid. The results of the BSVR model proposed showed little deviation compared to the experimental results. Applying backpropagation multilayered perceptron (MLP) artificial neural network, Hassan and Banerjee [83], excellently predicted the specific heat of molten salt nanofluid.

While the exact model for accurate specific heat prediction is yet to be obtained, some outlines can be drawn from available experimental data. The specific heat of nanofluids depends on, the volume concentration of nanoparticles, the nature of the base fluid, and the temperature of the fluid. In water-based nanofluids, the specific heat tends to reduce with an increase in volume concentration of nanoparticles [84, 85].

3.4 Nanofluid Thermal Conductivity (k)

The thermal conductivity of nanofluids plays a crucial role in the development of an energy-efficient HTF. The nanofluid thermal conductivity is affected by the thermal conductivity of the nanoparticles, the thermal conductivity of the base fluid, size of the particle, etc. Maxwell using the effective medium theory proposed the initial numerical model (Eq. 26) to determine the thermal conductivity of particles dispersed in a fluid [46, 86]:

$$\frac{k_{eff}}{k_{bf}} = \frac{k_p + 2k_{bf} + 2\varphi(k_p - k_{bf})}{k_p + 2k_{bf} - \varphi(k_p - k_{bf})}, \tag{26}$$

where k_{eff} represents the effective thermal conductivity, k_p is the thermal conductivity of the nanoparticle and k_{bf} is the thermal conductivity of the base fluid.

While the effective medium theory has been effective in predicting spherical dispersion of microparticles in fluids, it has been unable to accurately predict nanoparticle dispersion in fluids. Many other researchers have proposed formulas to predict the thermal conductivity of nanofluids more accurately by improving on Maxwell's initial formula. Accounting for particle shape, both Hamilton and Crosser's study [87] and Xuan and Li's study [88] modified Maxwell's model. Also, Yu and Choi improved on Maxwell's model by applying the superposition principle of series and parallel thermal conductivity [89]. Considering the effects of size, aggregation, surface absorption of particles, and applying fractal theory Wang et al. [90] proposed a different model for the numerical prediction of thermal conductivity. Yang [91] proposed a model that considered the Brownian motion and kinetic theory of nanoparticles.

Early results from Said et al. [92] experiment with Al_2O_3 water nanofluid and Murshed et al. [93] experiment with SiO_2 water nanofluid show that the classical models for predicting the thermal conductivity of nanofluids deviate significantly from experimental results. This deviation in prediction is increased in hybrid nanofluids as compared to conventional nanofluids [94, 95]. The studies by Taherialekouhi et al. [94] and Wole-Osho et al. [95] also show that regression correlation models within the range of the experiments conducted have less deviation than the classical models. The most accurate prediction models are correlation models

enhanced with artificial neural networks (ANN). Table 2 shows specific studies for nanofluid thermal conductivity models.

3.5 Nanofluid Viscosity

Another important property of nanofluids is viscosity; the viscosity of fluids influences their heat transfer performance. Einstein [109] was first to postulate the viscosity behavior of "small rigid spheres suspended in a liquid", he proposed Eq. 27, postulating that the coefficient of internal friction rises by a value which is equal to 2.5 times the total volume of the spheres suspended in a unit volume, provided that this total volume is less than 0.0245 [109]:

$$\frac{\mu_{eff}}{\mu_f} = 1 + 2.5\varphi, \tag{27}$$

where μ_{eff} is the effective viscosity, μ_f is the viscosity of the base fluid and $\varphi < 0.0245$.

However, like the classical models for thermal conductivity, numerical results obtained from the Einstein formula significantly underestimates the viscosity values when compared to experimental results. Many other researchers have proposed other numerical formulas. Mooney's classical model [110] improved on Einstein's work to increase the volume concentration range. The other classical and more recent models to predict effective viscosity are given in Table 3.

Some researchers, with the aid of experiments, have proposed numerical formulas for viscosity using correlation. Udawattha et al. [111] proposed a viscosity formula considering five effective variables. These variables include particle size, temperature, volume concentration, nanoparticle material, and particle shape. More recently, researchers have begun to do use computer-assisted models applying artificial intelligence (AI), artificial neural networks (ANN), and genetic algorithms (GA).

Radial basis function (BRF) neural networks have shown to better predict viscosity compared to other existing models [112]. Also, the Genetic Algorithms-Neural Network (GA-NN) model was used to predict viscosity in multiple water-based and glycol-based nanofluids, the GA-NN model, was shown to improve the viscosity modeling accuracy by 39% [113].

4 Application of Nanofluids in Solar Collectors

Nanoparticles within the nanofluids continuously undergo Brownian motion which leads to agglomeration. Agglomeration is a process whereby nanoparticles attract each other as they undergo Brownian motion. These interacting particles stick to each other and ultimately increase both the size and density of the nanoparticles [126]. The attraction force between these particles is known as the Van der Waals force [127]. London [128] theory postulates that the interaction energy (V_{int}) between molecules is directly proportional to the sixth power of the distance (R)

Table 2 Theoretical thermal conductivity models

Thermal conductivity numeric models		
Authors		Nanofluid
Classical models		
Maxwell model [46]	$\frac{k_{eff}}{k_f} = \frac{k_p+2k_f+2(k_p-k_f)\varphi}{k_p+2k_f-(k_p-k_f)\varphi}$	–
Bruggeman model [96]	$\varphi\left(\frac{k_p-k_{eff}}{k_p+2k_{eff}}\right)+(1-\varphi)\left(\frac{k_f-k_{eff}}{k_f+2k_{eff}}\right)=0$	–
Hamilton–Crosser model [87]	$k_{eff} = \frac{k_p+(n-1)k_f-(n-1)(k_f-k_p)\varphi}{k_p+(n-1)k_f+(k_f-k_p)\varphi}k_f$ where: $n = \frac{3}{\psi}$	–
Wasp model [97]	$\frac{k_{eff}}{k_f} = \frac{k_p+2k_f-2\varphi(k_f-k_p)}{k_p+2k_f-\varphi(k_f-k_p}$	–
Correlation model		
Esfe et al. [98]	$\frac{k_{nf}}{k_{bf}} = 0.999+9.58*10^{-5}T+0.00142T\varphi+0.0519\varphi^2+0.00208\varphi^4$	EG-based conventional
Nabil et al. [99]	$\frac{k_{nf}}{k_{bf}} = 1+(\frac{\varphi}{100})^{5.5}+(\frac{T}{80})^{0.01}$	Water/EG-based hybrid
Afrand [100]	$\frac{k_{nf}}{k_{bf}} = 0.8341+1.1\varphi^{243.5}T^{-0.289}$	EG-based hybrid
Esfahani et al. [101]	$\frac{k_{nf}}{k_{bf}} = 1+0.0008794\varphi^{0.5899}T^{1.345}$	Water-based hybrid
Wei et al. [102]	$\frac{k_{nf}-k_{bf}}{k_{nf}} = 0.00443+0.02636\varphi$	Diathermic oil-based conventional
ANN models		
Mehrabi et al. [103]	Genetic algorithm–polynomial neural network (GA-PNN) model	Water-based conventional
Esfe et al. [104]	Feedforward multilayer perceptron artificial neural network (MLP-ANN)	Water–EG-based hybrid
Vakili et al. [105]	Feedforward backpropagation artificial neural network (FFBP-ANN)	Water–EG-based conventional
Komeilibirjandi et al. [106]	Group method of data handling (GMDH-ANN)	Water-based conventional, engine oil-based conventional
Wole-Osho et al. [95]	Backpropagation ANN, ANFIS	Water-based hybrid
Shahsavar et al. [107]	Group method of data handling type neural network (GMDH-ANN)	Liquid paraffin-based conventional
Khalifeh and Vaferi [108]	Cascade feedforward backpropagation (CFB)	–

– Applicable to multiple nanofluids

between them. Therefore, in nanofluids, interaction energy increases with a rise in nanoparticle volume concentration [128]:

$$V_{int} = \frac{\upsilon}{R^6}, \tag{28}$$

where "υ" is a constant of proportionality.

Base fluids with high viscosity make more stable nanofluids because agglomeration happens less within highly viscous fluids. However, increase viscosity reduces heat transfer fluids [129]. As outlined, agglomeration affects the stability of the nanofluid. Therefore, nanofluid stability requires that the nanoparticles do not aggregate at a high rate. An easy way to improve the stability of a nanofluid is by the addition of a surfactant (dispersant). These additives change the transport properties of the nanofluids such as the thermal conductivity and viscosity which reduces heat transfer of nanofluids [130]. Due to the negative effect of adding dispersant to nanofluids, especially in heat transfer applications, some other techniques have been prescribed to improve on nanofluids stability without surfactant addition. Yang and Liu [131], presented a stable technique to prepare nanofluids; the technique showed no deposition layer even after boiling. Also, Hwang et al. [132] prepared nanofluids by the wet mechanochemical reaction, and the nanofluids showed low viscosity, high stability, and high thermal conductivity properties.

The remainder of this section investigates numerical and experimental studies of nanofluids applied in various solar thermal collectors.

4.1 Nanofluids in Flat Plate Collectors

Flat plate collectors are heat exchangers that convert energy from solar irradiation to useful thermal energy. To increase the thermal efficiency of the FPC, researchers aim to decrease the heat loss in from system reduces thereby increasing the useful energy gained from the system. Improving the heat transfer properties of the working fluid can increase useful energy gained from the system. Nanofluids have improved heat transfer properties over conventional working fluids. Several studies have been done to experimentally study the effects of using nanofluids as working fluids in FPC.

Figure 6 represents the experimental configuration for measuring the thermal performance of fluids in a flat plate collector system. All experiments of this nature are like the above experimental setup with only minor alteration. These configurations allow a dependable control of the mass flow rate and reliable measurement of ambient temperature, inlet temperature, and outlet temperature. All these variables are important to the determining heat removal factor, heat loss coefficient, and overall system efficiency.

Said et al. [133] observed the effects of using Al_2O_3 water-EG (60:40) nanofluid, at concentrations of 0.05% and 0.1%, as heat transfer fluids in a flat plate collector. The results showed alumina nanofluid at 0.05% exhibited Newtonian behavior at temperatures below 40 °C, but when volume concentration was 0.1% the nanofluid exhibited non-Newtonian behavior. Also, the thermal conductivity improved

Table 3 Theoretical models for nanofluids viscosity

Viscosity numerical models		
Authors		Nanofluid
Classical models		
Einstein model [109]	$\frac{\mu_{eff}}{\mu_f} = 1 + 2.5\varphi$	–
Mooney model [110]	$\frac{\mu_{eff}}{\mu_f} = e^{\frac{2.5\varphi}{1-k\varphi}}$	–
Krieger–Dougherty model [114]	$\frac{\mu_{eff}}{\mu_f} = 1 - \frac{\varphi}{\varphi_m}^{-2.5\varphi_m}$	–
Nielsen power-law model [97]	$\mu_{eff} = (e^{\frac{\varphi}{1-\varphi_m}}).\mu_f$	–
Batchelor model [115]	$\mu_{eff} = (1 + 2.5\varphi + 6.5\varphi^2)\mu_f$	–
Correlation model		
Abu-Nada [116]	$\mu_{\mathrm{nf}} = -0.155 - \frac{19.582}{T} + 0.794\varphi + \frac{2094.5}{T^2} - 0.192\varphi^2 - 8.11\frac{\varphi}{T}$	Water-based conventional
Hosseini et al. [117]	$\frac{\mu_{nf}}{\mu_{bf}} = \exp[m - \propto \left(\frac{T}{T_o}\right) + \beta(\varnothing_h) + \gamma(\frac{d}{1+r})]$	Water-based conventional
Esfe et al. [118]	$\frac{\mu_{nf}}{\mu_{bf}} = 0.9118exp(5.49\varphi - 0.0000136T^2 + 0.0303Ln(T)$	EG-based conventional
Azmi [119]	$\frac{\mu_{nf}}{\mu_{bf}} = \left(1 + \frac{\varnothing}{100}\right)^{11.3}\left(1 + \frac{T_{nf}}{70}\right)^{-0.038}(1 + \frac{d}{170})^{-0.061}]$	Water-based conventional
Asadi and Asadi [120]	$\mu_{\mathrm{nf}} = 796.8 + 76.26\varphi + 12.88T + 0.7695\varphi T - \frac{196.9T - 16.53\varphi T}{\sqrt{T}}$	Engine oil-based hybrid
Zawawi et al. [121]	$\frac{\mu_{nf}}{\mu_{bf}} = \left(1 + \frac{\varnothing}{100}\right)^{37}(1 + R)^{-0.02}(1 + \frac{T}{80})^{0.03}$	PAG-based hybrid
ANN models		
Sharifpur et al. [122]	Group method of data handling (GMDH-ANN)	EG-based conventional
Heidari [123]	Multilayer perceptron artificial neural network (MLP-ANN)	Conventional
Adio et al. [124]	Fuzzy C-means clustering-based adaptive neuro-fuzzy inference system (FCM-ANFIS)	EG-based conventional
Esfe et al. [125]	Multilayer perceptron artificial neural network (MLP-ANN	Engine oil-based hybrid

– Applicable to multiple nanofluids

compared to the conventional base fluid. However, the study also raised concerns about the viability of nanofluids as HTF in flat plate collectors because of the hysteresis phenomenon [134] observed in the fluid.

Several other studies have investigated the effect of nanofluid volume concentration on the thermal and exegetic efficiencies of flat plate collectors. Using silicon dioxide nanofluid at volume concentrations of 0.2% and 0.4%, Faizal et al. [135] observed that SiO_2 water nanofluid at 0.2% concentration was more efficient than SiO_2 water nanofluid at 0.4% volume concentration. The thermal efficiency of the solar collector increased by 23.5% when SiO_2 water nanofluid concentration was 0.2%. However, Meibodi et al. [136] also investigating SiO_2 nanofluid with a volume concentration of 0.5%, 0.75%, and 1%, observed that increase in nanofluid concentration from 0.5 to 1% results in efficiency enhancement between 4% and 8%. This enhancement was significantly less than the 23% enhancement observed when volume concentration was much lower at 0.2%. An essential point to note is that the base fluid and the particle size of SiO_2 used in Faizal et al. [135] experiment, is different from those used in Meibodi et al. [136] experiment; this can also explain the significant difference in results. Further investigation into the effect of volume concentration on the thermal efficiency of a flat plate collector was done using CuO–water nanofluid at 0.1% and 0.2% volume concentration [137]. The study found that thermal efficiency enhancement was 5% higher when nanofluid volume concentration was 0.1% compared to when volume concentration was 0.2%. The effects of the volume concentration (0.0%–1.5%) of MgO water nanofluid on the thermal efficiency of FPC was investigated by Verma et al. [138]. The experiment observed that within the volume concentration range considered, the FPC thermal efficiency gradually increased when volume concentration increased between 0.25% and 0.75%. However, the collector thermal efficiency reduced as volume concentration increased from 0.75% to 1.5%. MWCNT water nanofluid at volume concentrations of 0.01%, 0.05% and 0.1% was used to analyze energy and exergy efficiency in FPC. This research observed maximum efficiency enchantment of 34.2% at a nanofluid volume concentration of 0.1% [15]. As seen in Table 4, multiple experiments have investigated the effect of volume concentration on collector efficiency. It is safe to say, barring unique scenarios, an increase in nanofluid particle volume concentration would increase flat plate collector efficiency until volume concentration reaches an optimum value where further increase in volume concentration would not lead to an increase in collector efficiency. Also, the increase in volume concentration increases the viscosity of the nanofluid which limits the flow properties of the nanofluid.

In FPC analysis, several researchers have studied the effect of the nanofluid mass flow rate on the flat plate collector efficiency. Within the collector, the mass flow rates of 1, 2, and 3 $kg{\cdot}min^{-1}$ were applied to the CuO water nanofluids at a volume concentration of 0.4%; Moghadam et al. [139] observed maximum thermal efficiency improvement of 17% when collector mass flow rate was 1 $kg{\cdot}min^{-1}$. The results are unique in that flat plate collector efficiency appears to drop as CuO nanofluid mass flow rate rises. However, in more recent studies, the reverse appears to be the case. When SiO_2 water nanofluid was applied in the FPC, the efficiency of the collector increased when the flow rate increased: in the experiment mass flow

rate was varied between 0.35 kg·min^{-1} and 2.8 kg·min^{-1} [140]. Similar results were observed in Salavati Meibodi et al. [141] work. Studies from both Sharafeldin, Gróf, and Stalin et al. [142, 143] showed that within the mass flow rate range considered cerium dioxide water nanofluid performed better as the mass flow rate increased. The effect of mass flow rate on FPC efficiency was also observed by Sharafeldin et al. [144] using WO_3 water nanofluids; results show that WO_3 water nanofluid performed better as the mass flow rate increased, also, the efficiency of solar collector could reach about 71.87%.

From Table 4, most studies observe that thermal efficiency rises when the mass flow rate of the nanofluid within the collector increases. However, it is important to note that the optimum mass flow rate in the flat plate collector is dependent on the nanofluid fluid thermal characteristics.

Studies have suggested that because of the unique role of particle size in determining the thermal properties of the nanofluid. An optimum particle size base fluid combination exists. Said et al. [145] considered the effect of particle size on the thermal efficiency of the flat plate collector using Al_2O_3 water nanofluid synthesized with a particle size of 13 nm and 20 nm. The research recorded that the smaller size of nanoparticles has improved stability, thermal conductivity, energy, and exergy efficiencies. He et al. [137] also considered a similar experiment using CuO–water nanofluid at particle sizes of 25 nm and 50 nm to investigate the efficiency enhancement of FPC. Comparing the difference in thermal conductivity of nanofluid using different particle sizes of 25 nm and 50 nm. They found that the thermal conductivity in 25 nm CuO–water nanofluid is higher than that of 50 nm CuO–water nanofluid.

As outlined earlier, stability is an important factor that influences the nanofluid thermal properties. As the lack of nanofluid stability tends to affect their application. Michael and Iniyan [146] investigated the performance of CuO water nanofluid in the FPC water heating system under natural and forced circulation. The experiment showed that sodium dodecyl benzene sulfonate (SDBS) was a better surfactant than Triton X-100 after 3 days of stability test. It is vital to identify that there was a significant improvement in performance in thermosyphon flow compared to forced flow. Varying dispersant volume concentration between 0.2% and 0.4%. Kiliç et al. [147] investigated the effect of dispersant volume concentration on the FPC thermal efficiency. Water absorption TiO_2 water nanofluid was applied as a heat transfer fluid. The nanofluid had the least agglomeration when dispersant concentration was 0.2%.

Using HCl and NaOH, Yousefi et al. [148] varied the pH of the MWCNT water nanofluid. Three different pH values (3.5, 6.5, and 9.5) were considered, to determine the effect of pH on FPC thermal efficiency. The experiment observed that as nanofluid became either more acidic or more basic the efficiency of the collector improved. The isoelectric point (where molecules carry no electrical charge) explains this phenomenon in the fluid. The larger the difference between the fluid pH and the isoelectric point, the more efficient the working fluid [149]. The challenge with this is that the most stable pH values will tend to corrode the risers and tanks of most collector systems.

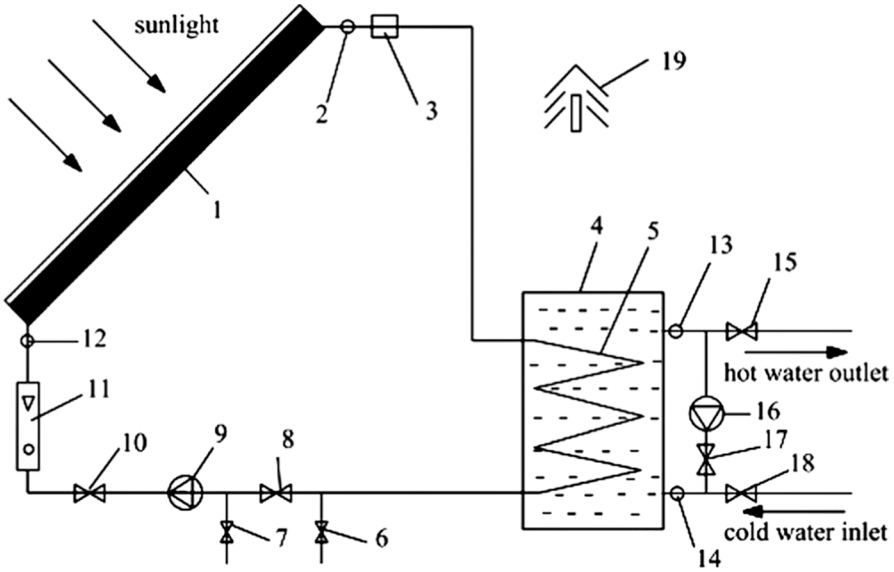

***1-Solar collector; 2,12,13, 14 - thermocouple 3- vent valve; 4- fluid tank; 5- heat exchanger; 6,7,8,10,15,17,18-valve; 11-flowmeter; 9,16 water pump; 19- thermometer

Fig. 6 Diagram of the experimental setup to measure useful energy

Collecting solar radiation values from sunrise to sunset, the exergy efficiency optimization was studied when solar radiation (G_t) and ambient temperature (T_a) parameters are dynamic [150]. The experiment observed minimum solar irradiation to be 187 $W{\cdot}m^{-2}$ and maximum solar radiation values to be 1087 $W{\cdot}m^{-2}$. The results show that optimum exergy efficiency decreases exponentially with increasing T_a/G_t value.

Carbon nanomaterials are naturally black, making these materials natural thermal absorbers. Carbon also has high thermal conductivity making carbon-based nanofluids very efficient heat transfer fluids [151]. In literature, there have been 3 unique carbon allotropes that have been used as FPC heat transfer nanofluids. These carbon allotropes include graphene, single-wall carbon nanotubes (SWCNTs), and multi-wall carbon nanotubes (MWCNTs), as seen in Fig. 7.

Since minimizing entropy generation helps maximize useful energy output. SWCNTs based nanofluid can be very useful for higher temperature systems. An experiment using SWCNT water nanofluid at a volume concentration of 0.3% and 0.1% as the HTF in a flat plate collector was conducted by Said et al. [152]. In the experiment, the highest exergy efficiency measured for distilled water when the mass flow rate was 0.5 $kg{\cdot}min^{-1}$ is 8.77% while exergy efficiency was enhanced up to 26.25% and 22.35% for 0.3% and 0.1% volume concentration of SWCNTs nanofluid under similar conditions.

Graphene water-based nanofluid at a volume concentration of 0.01% and 0.02% was used to evaluate the thermal performance of a flat plate collector [153]. It is

relevant to point out that in this study, stability was vastly improved without surfactant but by increasing the nanofluid pH to 11.6. The results showed that compared to deionized water, the thermal efficiency of the FPC increased by 12.19% when graphene water nanofluid at 0.01% volume concentration was used. When volume concentration increased from 0.01% to 0.02%, a further efficiency improvement of 6% was achieved. Said et al. [154] also numerically investigated the exergetic efficiency of FPC using graphene water nanofluids as the working fluid. The research found that increasing nanoparticle volume concentration increased exergy efficiency. The analyses also revealed that by using graphene water nanofluid exergy efficiency can be enhanced by 21%. Six different nanofluids were compared to determine the most efficient in FPC. These nanofluids include aluminum oxide (Al_2O_3) water nanofluid with average nanoparticle (NP) size of 45 nm, titanium oxide (TiO_2) water nanofluid with average NP size of 44 nm, silicon oxide (SiO_2) water nanofluid with average nanoparticle NP size of 10 nm, copper oxide (CuO) water nanofluid with average nanoparticle NP size of 42 nm, graphene water nanofluid with average NP size of 20 nm, and multiwalled carbon nanotubes (MWCNTs) water nanofluid with NP aspect ratio 200 and external diameter of 7 nm [155]. The results can be seen in Fig. 8.

While water has the highest specific heat, it has the least density, viscosity, and thermal conductivity. CuO water nanofluid is highly viscous and the densest of the considered nanofluid at the volume concentration range between 0.25% and 2.0% [155].

In a study by Verma et al. [155], among the metal oxide nanofluids considered, CuO water nanofluid improved FPC efficiency the most. However, when the metal oxides nanofluids are compared to the carbon-based nanofluids, the carbon-based nanofluids are more efficient working fluids; this can be seen in Fig. 9.

As observed in Fig. 8, conventional nanofluids do not always possess all the desirable properties required during application. Some conventional nanofluid may have desirable thermal properties however lack desirable rheological characteristics. Hybrid nanofluids can be created to improve the application properties of nanofluids. Verma et al. [156] considered CuO–MWCNT hybrid nanofluid and MgO–MWCNT nanofluid as working fluid in FPC. The mixture ratio of the metal oxide to the MWCNT in the hybrid nanofluid was 4:1, respectively, for both nanofluids. 4MgO–MWCNT–H_2O and 4CuO–MWCNT–H_2O hybrid nanofluid have better efficiency performance than both CuO water nanofluid and MgO water nanofluid. However, MWCNT/water still performs better than all the hybrids at the optimum volume concentration of 0.75% and the mass flow rate of 2.1 $kg{\cdot}min^{-1}$. Among the hybrid nanofluids, 4MgO–MWCNT–H_2O hybrid nanofluid outperforms 4CuO–MWCNT–H_2O as a working fluid in a flat plate collector; even though CuO water nanofluid outperforms MgO water nanofluid when compared as FPC working fluids. While the hybrid nanofluid did not outperform the conventional nanofluid in Verma et al. [155] experiment, further investigation into nanofluid particle mixture ratios effect on flat plate collector efficiency needs to be done, as unique behaviors have been observed in the thermophysical studies of hybrid nanofluids [157, 158]. Similar results were obtained by Okonkwo eta al. [26], where the thermal efficiency of the FPC was enhanced by 2.6% when using alumina water nanofluids which

Table 4 Studies on the use of nanofluids in flat plate solar collectors

Author	Base fluid	Preparation method	Particle material	Particle size	Dispersant	Volume concentration (%)	Storage Tank	Mass Flow rate ($kg \cdot min^{-1}$)	Absorption Area(m2)	Result highlights
Said et al. 2013 [92]	Water/ethylene glycol	Two-step method	Al_2O_3	13	Not applicable	0.05%—0.1%	No	1.0,1.5, 2.0,2.5, 3.0	1.51	Al_2O_3 dispersed water/ethylene glycol Nanofluids have greater thermal conductivity than conventional base fluids. The nanofluid viscosity increases with an increase in volume concentration. However, the viscosity decreases exponentially with a linear increase in temperature
Shojaeizadeh and Veysi 2016 [150]	Water	Two-step method	Al_2O_3	15	Sodium dodecylbenzenesulfonate (SDBS)	0.4462%, 0.7383%, 0.9267%	No	0.2, 0.3, 0.4	1.51	Maximum exergy efficiency and optimum values of mass flow rate and volume concentration parameters follow an exponential trend with solar radiation/ambient temperature values. The parameters optimized and the optimum exergy efficiency is of a linear relationship with each other

Table 4 (continued)

Author	Base fluid	Preparation method	Particle material	Particle size	Dispersant	Volume concentration (%)	Storage Tank	Mass Flow rate ($kg \cdot min^{-1}$)	Absorption Area(m2)	Result highlights
Moghadam et al. 2014 [139]	Water	Two-step method	CuO	40	Not applicable	0.4%	No	1, 2, 3	1.51	The optimum mass flow rate is dependent on the working fluid thermo-physical characteristics. When compared with CuO–H_2O increased the STC efficiency compared with water by 16.7% (at considered optimum flow rate)
Michael and Iniyan 2015 [146]	Water	Two-step method	CuO	75	Sodium dodecylbenzene sulfonate (SDBS)	0.05%	Yes	6	Not Available	Sodium Dodecyl Benzene Sulfonate (SDBS) was a better surfactant than Triton X-100 after 3 days stability test. CuO water nanofluid at a concentration of 0.05% improved the thermal efficiency of the solar water heater by 6.3%. Efficiency in FPC improves with the rise in mass flow rate in a range between 0.01 $kg \cdot s^{-1}$ to 0.1 $kg \cdot s^{-1}$

Table 4 (continued)

Author	Base fluid	Preparation method	Particle material	Particle size	Dispersant	Volume concentration (%)	Storage Tank	Mass Flow rate ($kg \cdot min^{-1}$)	Absorption Area(m2)	Result highlights
He, Zeng, and Wang 2014 [137]	Water	Two-step method	CuO	25	SDBS	0.1%,0.2%	No	2.33	2	Thermal conductivity in 25 nm CuO water nanofluid is higher than that of 50 nm CuO water nanofluid. The effect of volume concentration using 25 nm CuO water nanofluid at 0.1% and 0.2%. However, the volume concentration at 0.1% has higher efficiency
Mirzaei 2019 [159]	Deionized water	Two-step method	CuO	40	Not applicable	0.1%	Yes	1, 2, 4	1.51	The average value for the collector efficiency enhancement of 15.2%, 17.1%, and 55.1% has been observed for 1, 2, and 4 $L \cdot min^{-1}$ flow rate of nanofluid, respectively. Unsteady conditions occur at lower flow rates, meanwhile increasing the flow rate subsequently lowers residence times of working fluid, therefore working fluid approach to steady conditions

Table 4 (continued)

Author	Base fluid	Preparation method	Particle material	Particle size	Dispersant	Volume concentration (%)	Storage Tank	Mass Flow rate ($kg \cdot min^{-1}$)	Absorption Area(m2)	Result highlights
Verma, Tiwari, and Chauhan 2016 [138]	Double distilled water	Two-step method	MgO	40	Not applicable	0.25%,0.5%, 0.75%.1.0%, 1.25%,1.5%	No	0.5,1, 1.5, 2.0, 2.5, 3.0	0.375	Optimum volume concentration is 0.75% within the considered range. Maximum efficiency enhancement was 9.34% in FPC recorded for mass flow rate at 1.5 lpm and 0.75% particle volume concentration compared to water for same flow rate
Faizal et al. 2015 [135]	Distilled water	Two-step method	SiO_2	15	Not applicable	0.2%, 0.4%	No	1.0, 1.5, 2.0, 3.0	1.84	Silicon dioxide nanofluid can improve thermal collector efficiency by 23.5%. This can provide environmental advantages of; reducing CO_2 emission and copper and the glass material used in the FPC

Table 4 (continued)

Author	Base fluid	Preparation method	Particle material	Particle size	Dispersant	Volume concentration (%)	Storage Tank	Mass Flow rate ($kg \cdot min^{-1}$)	Absorption Area(m2)	Result highlights
Salavati Meibodi et al. 2015 [141]	Water/ethylene glycol	Two-step method	SiO_2	40	Not applicable	0.5%, 0.75%, and 1%	No	1.08, 1.92, 2.7	1.59	Thermal efficiency is improved by up to 63% in nanofluid with SiO_2 particles dispersed in EG/water base. When volume concentration is between 0 and 1% the maximum change in efficiency is between 4% and 8%. Hence considering the trade-off between preparation and stability against efficiency gain. It may be better to use a lower volume fraction

Table 4 (continued)

Author	Base fluid	Preparation method	Particle material	Particle size	Dispersant	Volume concentration (%)	Storage Tank	Mass Flow rate ($kg \cdot min^{-1}$)	Absorption Area(m2)	Result highlights
Noghrehabadi, Hajidavaloo, and Moravej 2016 [140]	Water	Two-step method	SiO_2	12	Not applicable	1%	No	0.35, 0.7, 1.05, 1.4, 1.75, 2.1, 2.45, 2.8	1	The SiO2/water nanofluid increased the efficiency of the square flat plate solar collector compared with net water. An increase in solar radiation has no apparent effect on the efficiency of the collector. However, for the nanofluid, the efficiency of the collector was increased with a very low slope by increasing the incident solar radiation. The efficiency of the square flat plate solar collector was increased by increasing the mass flow rate
Kiliç, Menlik, and Sözen 2018 [147]	Deionized water	Two-step method	TiO_2	44	Triton X-100	0.02%	No	1.98	1.64	The performance increase in collector has a maximum instantaneous efficiency is between 34.43%. When dispersant concentration was varied between 0.2% and 0.4% results show that nanofluid had the least agglomeration when dispersant concentration was 0.2%

Table 4 (continued)

Author	Base fluid	Preparation method	Particle material	Particle size	Dispersant	Volume concentration (%)	Storage Tank	Mass Flow rate ($kg{\cdot}min^{-1}$)	Absorption Area(m2)	Result highlights
Said et al. 2015 [152]	Distilled water	Two-step method	SWCNTs	*l* = *1-3* µm, *d* = *130* nm	Sodium dodecyl sulfate	0.1%,0.3%	No	0.5	1.84	Maximum conductivity enhancement of 91% is obtained at a temperature of 323 K for 0.3 vol.% volume fraction, whereas the minimum enhancement in conductivity is 12% for 0.1 vol.% volume fraction of SWCNTs at 298 K in comparison with water. An increase in viscosity is observed with the increasing volume fraction of SWCNTs and surfactants. The entropy generation is 32.21 M/K for 0.1 vol.% SWCNTs, for a mass flow rate of 0.5 $kg{\cdot}min^{-1}$ while entropy generation is 43.53 M/K for water with a similar mass flow rate. The maximum energy efficiency in FPC is about 95.12% using the nanofluid and efficiency was 42.07 when water was used. exergy efficiency with SWCNT is close to 26.25% compared to water which was 8.77%

Table 4 (continued)

Author	Base fluid	Preparation method	Particle material	Particle size	Dispersant	Volume concentration (%)	Storage Tank	Mass Flow rate ($kg \cdot min^{-1}$)	Absorption Area(m2)	Result highlights
Ahmadi, Ganji, and Jafarkazemi 2016 [153]	Deionized water	Two-step method	Graphene	100	Not applicable	0.01%, 0.02%	No	0.16	Not Available	Kinematic viscosity reduces with rising temperature in a liquid state. Thermal efficiency is increased by 12.19% when 0.01 wt% Graphene/water nanofluid was used compared to water deionized water. When volume concentration is increased from 0.01% to 0.02% a further 6% in efficiency improvement can be gained
Said et al. 2014 [160]	Deionized water	Two-step method	SWCNTs	–	Not applicable	0.02% -0.034%	No	Not Available	1.51	SWCNTs based nanofluids have better thermal properties and improved thermal and exergetic efficiencies compared to water. SWCNT nanofluid reduces the entropy generation by 4.34% and enhances the heat transfer coefficient by 15.33% theoretically compared to water as an absorbing fluid
Yousefi et al. 2012 [161]	Double distilled water	Two-step method	MWCNTs	D = 10–30 nm	Triton X-100	0.2%	No	2	1.51	pH modulation of the nanofluid can improve nanofluid stability which in turn improves thermal efficiency enchantment of the FPC

Table 4 (continued)

Author	Base fluid	Preparation method	Particle material	Particle size	Dispersant	Volume concentration (%)	Storage Tank	Mass Flow rate ($kg \cdot min^{-1}$)	Absorption Area(m2)	Result highlights
Eltaweel and Abdel-Rehim 2019 [15]	Distilled water	Two-step method	MWCNTs	*l* = *20* µm, *d* = *10–40 nm*	Not applicable	0.01%, 0.05% and 0.1%	No	0.5, 1, 1.5	2	0.01 wt%, 0.05 wt%, and 0.1 wt% MWCNTs increased the efficiency by 16% 21%, and 34.13%, respectively, compared with the efficiency attained using distilled water. The maximum exergy efficiency for the flat plate solar collector is approximately 23.35% compared to what is achieved with distilled water
Sharafeldin and Gróf 2018 [142]	Deionized water	Two-step method	CeO_2	25	Not APPLICABLE	0.0167%, 0.033%, 0.066%	No	0.9,1.08,1.14	1.78	Various volume fractions (0.0167, 0.0333, and 0.0666) were tested at mass flow rates between 0.015 and 0.019 $kg \cdot s^{-1}$. The efficiency of the collector was directly proportional to the mass flow rate, and it seemed that an optimal volume concentration of 0.0333% within the range of values studied

Table 4 (continued)

Author	Base fluid	Preparation method	Particle material	Particle size	Dispersant	Volume concentration (%)	Storage Tank	Mass Flow rate ($kg \cdot min^{-1}$)	Absorption Area(m2)	Result highlights
Mahmoud Ahmed Sharafeldin, Gróf, and Mahian 2017 [144]	Distilled water	Two-step method	WO_3	90	Not applicable	0.0167%, 0.033%, 0.066%	No	0.936,1.098, 1.17	1.78	Efficiency enhancement is dependent on the mass flow rate, volume concentration, and the reduced temperature parameter. The maximum efficiency of the solar collector was 71.87% for a volume fraction of 0.0666% and a mass flux rate of 0.0195 $kg \cdot s^{-1}$ within the studied range
Verma, Tiwari, and Chauhan 2017 [155]	Double distilled Water	Two-step method	CuO, SiO_2, TiO_2, Al_2O_3, Graphene, MWCNTs	CuO = 42 SiO_2 = 10 TiO_2 = 44 Al_2O_3 = 45 Graphene = 10 MWCNTs = (I = 20 µm, d = 7 nm)	Not applicable	0.75%	No	0.6, 1.14, 1.65, 2.1, 2.55, 3.0	0.375	Carbon-based nanofluids are the most efficient working fluids. CuO water nanofluid is the most viscous and most dense of the considered nanofluid at the volume concentration range between 0.25% and 2.0%

Table 4 (continued)

Author	Base fluid	Preparation method	Particle material	Particle size	Dispersant	Volume concentration (%)	Storage Tank	Mass Flow rate ($kg \cdot min^{-1}$)	Absorption Area(m2)	Result highlights
Verma et al. 2018 [156]	Water	Two-step method	4MgO–MWCNT 4CuO–MWCNT	MgO =, CuO =, MWCNTs = (I = 20 µm, d = 7 nm)	Not applicable	0.25%,0.5%,0.75%.1.0%,1.25%,1.5%, 2.0%	No	0.6, 1.14, 1.65, 2.1, 2.55, 3.0	0.375	In both 4MgO–MWCNTs/water hybrid and 4CuO–MWCNTs/water nanofluid, it was observed that thermal conductivity and viscosity increased as volume concentration increased between 0.00%-2.00%. 4MgO–MWCNTs/H2O is more thermally efficient than 4CuO–MWCNTs/H2O as working fluid in FPC

performed better than Alumina-iron water nanofluids with 1.79% enhancement in the FPC.

As previously stated when the metal oxides nanofluids are compared to the carbon-based nanofluids, the carbon-based nanofluids are more efficient working fluids. Therefore, it is becoming clearer that nanofluids containing the carbon allotropes have a significant advantage in heat transfer applications. However, since it is also becoming obvious that hybrid nanofluids outperform conventional nanofluids in improving the efficiency of the collectors. The exact nanofluid arrangement for optimum collector performance still requires further investigation.

4.2 Nanofluids in Evacuated Tube Collectors (ETC)

ETC is special in that the heat losses witnessed in flat plate collectors are minimized due to the presence of vacuum insulation. A vacuum exists between the outer glass glazing and the absorber medium of the evacuated tube. This vacuum acts as an insulation, which reduces the thermal losses due to convection and conduction. There are two main types of ETC: heat pipe-ETC and direct flow- ETC (U-tube ETC). From Fig. 3, the heat pipe-ETC contains a heat pipe that is attached to the absorber plate. These heat pipes contain antifreeze liquid enclosed within it. This heat pipe protrudes out of the glass cover into a heat exchanger called a manifold. U-tube ETC contains two heat pipes connected with a U-shaped pipe within (see Fig. 10). This U-shaped heat pipe connects adjacent ends: an inlet pipe allowing low temperature working fluids and an outlet pipe where heated working fluid exit.

The effect of using alumina nanofluid in heat pipe-ETC was investigated by Pise et al. [162]. Mixing Al_2O_3 nanoparticles (NP) with an average size of 50 nm in water using the two-step process; the synthesized nanofluid was used as a working fluid for the heat pipe-ETC tilt angles between 18.63° and 60°. The study observed that the collector efficiency rose as the tilt angle rose between 18.63° and 50° and begins to decrease further as the tilt angle rise between 50° and 60°. The increase in gravitational force as the title angle approached 90° causes an efficiency reduction within the heat pipe. Alumina nanofluid at a volume concentration of 0.05%, 0.1%, and 0.5% the thermal efficiency performance of the collector improved by 3.79%, 10.72%, and 15.24%, respectively, when compared to water under similar conditions. The experiment also observed that with an increase in nanofluid volume concentration, the thermal efficiency of the heat pipe-ETC improves.

Kim et al. [163] conducted a similar test using Al_2O_3 water nanofluid; in the experiments, the effects of particle size, volume concentration, and flow rate on the ETC's thermal efficiency were investigated. Considering particle sizes of 20 nm, 50 nm and 100 nm, volume concentration of 0.5%, 1.0% and 1.5%, mass flow rate of 1.98 $kg{\cdot}min^{-1}$ and 2.82 $kg{\cdot}min^{-1}$. The experiment recorded that thermal efficiency rose when volume concentration was between 0.5% and 1.0% and the collector efficiency was least when volume concentration was at 1.5%. The increase in nanoparticle size negatively affected the thermal efficiency of the collector, as nanofluid with 100 nm NP was less efficient than Al_2O_3 water nanofluid synthesized with 50 nm NP. Al_2O_3 water nanofluid synthesized with 20 nm NP recorded the highest

collector efficiency of 24.1% compared to water under similar conditions. As the mass flow rate changed between 1.98 kg·min^{-1} to 2.82 kg·min^{-1}, the efficiency of the collector dropped about 3%.

Ghaderian and Sidik [164] set up an experiment to investigate the energy efficiency performance of ETC using Al_2O_3 water nanofluid. This investigation done with a passive-glass circulation evacuated tube solar thermosyphon collector model, connected to a spherical coil inside a horizontal tank. Heat transfer occurs between the working fluid in the tank and the fluid moving within the coil. The nanofluid was synthesized by the two-step method using distilled water and Al_2O_3 NP with an average size of 40 nm at a volume concentration of 0.03% and 0.06%. It was observed that the temperature difference in the nanofluid was proportional to solar irradiation in the time between 9 am and 5 pm. The results show that the collector maximum efficiency improvement was 39.52% when Al_2O_3 water nanofluid was at 0.03% volume concentration. However, when volume concentration is increased to 0.06% the maximum efficiency improvement increased to 58.65%. Also, the thermal efficiency of the collector increases with an increase in mass flow rate between 0.33 kg·min^{-1} and 1 kg·min^{-1}.

Using CuO water nanofluid, the effects of particle size, volume concentration, and mass flow rate on the heat transfer performance of a U-Tube ETC was investigated by Kang et al. [32]. CuO water nanofluid was prepared using nanoparticles with an average size of 80 nm and 40 nm at a volume concentration of 0.1%, 0.3%, 0.5%, and 0.7%. Results show that under the same experimental conditions, CuO nanofluid with an average NP size of 40 nm performed better than CuO water nanofluid with an average NP size of 80 nm and water. Also, the efficiency of the collector improved as volume concentration increased from 0% (water) to 0.5%. However, no significant improvement in efficiency was noticed when the volume concentration of the nanofluid increased from 0.5% to 0.7%. For the considered mass flow rates, an increase in fluid flow rate improved the efficiency of the collector for both water and CuO water nanofluid.

The performance improvement of gravity assisted heat pipe-ETC using CuO–acetone and Al_2O_3–acetone nanofluid as working fluid within the heat pipe was investigated [165]. The experimental setup is displayed in Fig. 11, thermocouples are placed at even distances in the evaporation and condensation region. The sensors allow the measurement of the mean wall temperature in both regions. Using CuO–acetone nanofluids and Al_2O_3–acetone nanofluids and synthesized with NP average size of 25 nm and 20 nm, respectively. The experiment considered the effect of volume concentration, title angle, and liquid filling ratio within the heat pipe. In the experiment conducted, thermocouple recorded temperature change within both the condensation and evaporation region of the heat pipe. The experiment concluded that the optimal filling ratio was 70% within the range (40, 50, 60, 70, and 80%) considered. Studying the effects of liquid filling ratio, the experiment observed that mean wall temperature was maximum when the minimum filling ratio was 40% and the maximum filling ratio was 70%. The research also found that the optimal filling ratio was 70% and that increase filling ratio beyond optimal, increased thermal resistance in the liquid, this behavior can be explained by the geyser effect [166]. The heat transfer coefficient was enhanced by 36% using Al_2O_3–acetone nanofluid

at 0.25% volume concentration, however, when volume concentration increases to 0.5% heat transfer coefficient improved by 64%. Similarly, the heat transfer coefficient is enhanced by 24% when the volume concentration of CuO–acetone nanofluid increased from 0.25% to 0.5%. The research also estimated 45° as the optimum inclination angle.

An Experiment using TiO_2–water nanofluid combined with Polyvinylpyrrolidone (PVP) surfactant was used to analyze the entropy generation and energy efficiency of a heat pipe-ETC [167]. The volume concentration (0.1%, 0.3% and 0.5%), surfactant-NP ratio (3:1, 2:1 and 1:1) and sonication time (10 min, 20 min and 30 min) were varied in the experiment. The experiment observed that the thermal conductivity of the TiO_2–water nanofluid decreases with an increase in the PVP surfactant ratio this agrees with [168]. An increase in sonication time does not have any major effect on the thermal conductivity of the nanofluid at any volume concentration and an increase in volume concentration leads to higher thermal conductivity within the range considered. Using the optimally synthesized TiO_2–water nanofluid with volume concentration at 0.5% and surfactant ratio of 1:1 and 10 min sonication time. The experiment further observed that while the energy efficiency of heat pipe-ETC increased with the increase in mass flow rate (1.02 $kg{\cdot}min^{-1}$, 1.5 $kg{\cdot}min^{-1}$, and 1.98 $kg{\cdot}min^{-1}$) the entropy generation reduced with increasing flow rate. Mahendran et al. [169] also used TiO_2 water nanofluid to determine the efficiency enhancement of U-tube-ETC. The experiment detected that at all volume concentrations and flow rates the nanofluid had performed less efficiently than water under the same conditions. However, this result does not conform to existing literature, and no replica study has been done to confirm these results.

Sharafeldin and Gróf [170] experimented to determine the performance of ETC using CeO_2 water nanofluid as the working fluid. The fluid was conventionally synthesized by the two-step method using CeO_2 NPs with an average size of 25 nm at 0.015%, 0.025%, and 0.035% volume concentrations. The results showed that the temperature difference between fluid at the outlet pipe and fluid at inlet pipe increased as the mass flow rate increased from 0.78 $kg{\cdot}min^{-1}$ to 1.02 $kg{\cdot}min^{-1}$ for all concentrations of working fluids. Also, the increase in fluid NP concentrati1n increases the temperature difference between inlet and outlet pipes. Compared to water under similar conditions, the nanofluid maximum performance improvement was 37.3%.

Sharafeldin and Gróf [171] conducted another similar experiment using the WO_3 water nanofluid at a volume concentration of 0.014%, 0.028%, and 0.042% and synthesized with an average NP diameter of 90 nm. The results observed that the efficiency of the collector improved with an increase in volume concentration and an increase in flow rate within the studied range. The maximum efficiency reached was by the collector during the experiment was 72.83%, approximately 19.3% better compared to water under similar working conditions. Kaya et al. [172], experimentally investigated the efficiency of U-tube-ETC using ZnO/EG–water when volume concentration was 1%, 2%, 3%, and 4% and the base fluid was ethylene glycol water (1:1). Polyvinylpyrrolidone (PVP) surfactant was added to the nanofluid to reduce problems of nanofluid agglomeration, which can affect the stability of the fluid, especially at high concentrations [126]. Their study observed the average

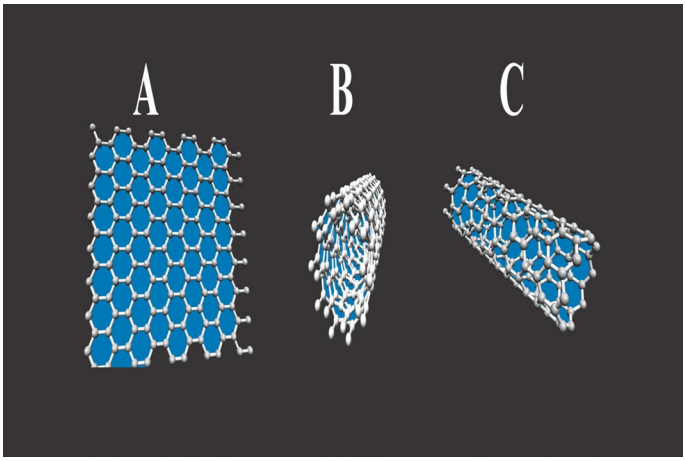

Fig. 7 Diagram of (a) grapheme, (b) MWCNT and (c) SWCNT

daily efficiency over five days and detected that they were no significant changes in efficiency which implied that no sedimentation occurred within the nanofluid over that period. The experiment also observed that though the collector efficiency improved with an increase in volume concentration from 1% to 3%, the collector efficiency reduces when volume concentration is further increased between 3 and 4%. The U-tube ETC collector efficiency improved as the mass flow rate increased within the considered range. The maximum collector efficiency enhancement of the U-tube ETC obtained was 62.87% with 3.0% ZnO EG–water nanofluid at a mass flow rate of 2.7 kg·min^{-1}. The thermal energy transfer property of SiO_2 water nanofluid within solar collector vacuum tubes was experimentally and numerically investigated by Yan et al. [173] The study recorded thermal conductivity and transmissivity measurement for the nanofluid at three-volume concentrations of 5%, 3%, and 1%. It observed that as volume concentration increased the thermal conductivity also improved. However, after 20 days of observation, the thermal conductivity performance of the nanofluid decrease under the same radiance condition, this was attributed to agglomeration. Results observed that transmissivity was better in nanofluids with a lower volume concentration of SiO_2 NP than nanofluids with higher volume concentration when the wavelength is observed within the visible and near-infrared spectrum. Numerically, it was simulated that the velocity of working fluid increased with an increase in volume concentration of SiO_2 nanoparticles. Ozsoy and Corumlu [174] designed a novel experiment to determine the thermal performance of a natural circulation heat pipe-ETC using Ag–water nanofluid. Ag–water nanofluid is synthesized by using the one-step chemical method proposed by Bulut and Özacar [175]. The experiment setup was similar to Fig. 11 with heat pipe -ETC placed at 35° angle of inclination conducted under controlled laboratory conditions to reduce variable external environmental influences. The mass flow rate within the heat pipe was 0.18 kg·min^{-1}. The results observed thermal conductivity of Ag–water nanofluid is directly depends on the temperature change. The experiment also observed

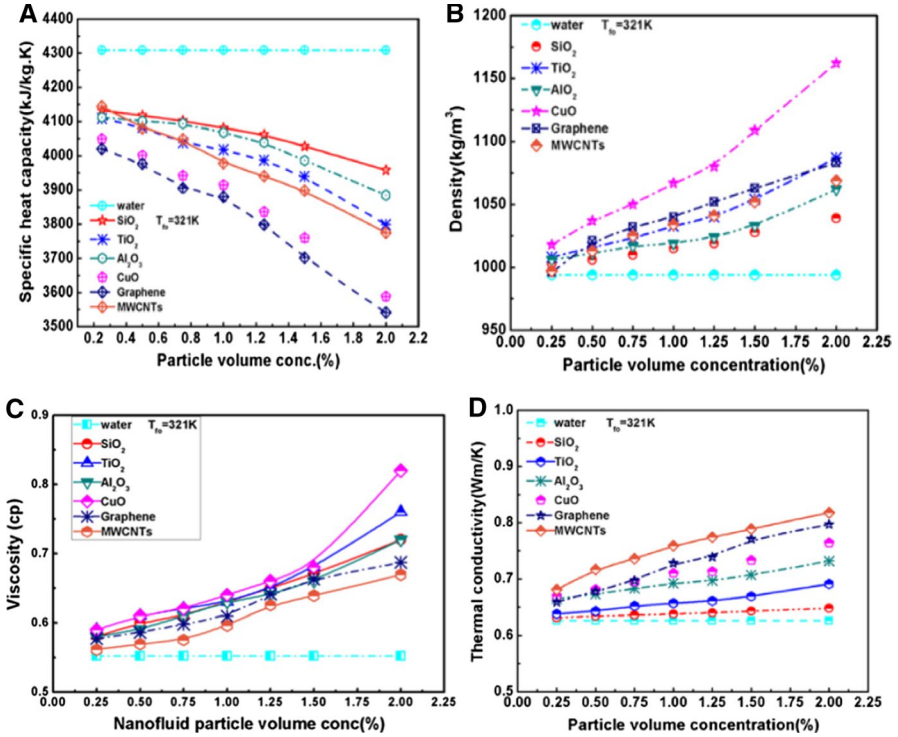

Fig. 8 (a) Specific heat versus volume concentration, (b) density versus volume concentration, (c) viscosity versus volume concentration, (d) thermal conductivity versus volume concentration [155]

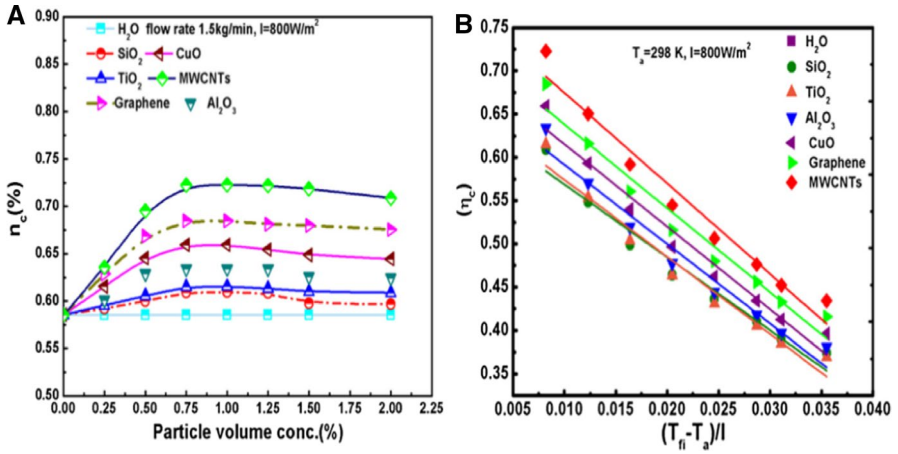

Fig. 9 (a) Collector efficiency and particle volume concentrations, (b) collector efficiency versus reduced temperature parameter [155]

that nanofluid absorption dropped by approximately 52% after one year. The temperature difference between the evaporator and condenser section was lower in the nanofluid than is with water under the same conditions. Efficiency in the collector was improved considerably compared to water.

Hussain et al. [176], experimentally studied the thermal efficiency performance of ETC using Ag water and ZrO_2 water nanofluids. The study considered volume concentrations at 1%, 3%, and 5% for both fluids. The experiment observed the thermal efficiency of the collector improved with an increase in mass flow rate and volume concentration. It also concluded that the solar collector efficiency using Ag water nanofluid was greater than ZrO_2 water nanofluid under the same conditions. However, the study did not determine if this was as a result of particle size difference or difference in the thermal conductivity of the considered particles.

An experiment was carried out to observe efficiency improvement in ETC using SWCNT water nanofluid in a roof-mounted U-tube-ETC with absorption area of approximately 42 m^2 and at an inclination angle of 25° [177]. The study observed that a maximum efficiency improvement of 10% using SWCNT–water nanofluid at 0.2% volume concentration as compared to water under the same conditions. Another carbon allotrope, grapheme–water nanofluid at 0.025%, 0.05%, 0.075% and 0.1% volume concentration (without surfactant) was used as working fluid in ETC [178]. The experiment observed that while thermal conductivity and viscosity increased with an increase in volume concentration, specific heat reduced with an increase in volume concentration. This study also observed that the collector efficiency increased as volume concentration and mass flow rate increased within the observed range. The maximum thermal efficiency recorded when the mass flow rate was 1.5 $kg{\cdot}min^{-1}$, and the volume concentration was 0.1% was 35.8% higher than in distilled water. Kim et al. [179] analyzed the theoretical efficiency of MWCNT, CuO, Al_2O_3, TiO_2, and SiO_2 in U-tube ETC. Assuming the heat transfer coefficient of the header of the tube to be constant and air convention negligible, the heat gain by the tube was modeled. Using propylene glycol water (1:5) as base fluid. The study concluded that MWCNT was the most efficient working fluid for the U-tube ETC and was 39% more efficient than water. The ETC efficiency increased by about 0.52% on average as the volume concentration of nanofluids increased from 1 vol% to 2 vol% for the metal oxides. However, the same increase was noticed in MWCNT nanofluid when volume concentration increased from 0.1 vol% to 0.15 vol%.

Table 5 shows some other studies and the conclusions reached on the effects of nanofluids in ETC. The volume concentration of the nanofluid plays an important role in the thermal efficiency of the ETC. It can be stated that like the flat plate collectors, the nanofluid's particle volume concentration would increase the ETC efficiency until volume concentration reaches an optimum value. Also, an increase in the mass flow rate tends to increase ETC thermal efficiency. Thermal efficiency also tends to increase with an increase in the filling ratio of the heat pipe, but filling ratio also has an optimum value. More experiments are necessary to investigate the effect of hybrid nanofluid on the evacuated tube collectors' performance. Also as is the case with FPC, nanofluids containing carbon have shown in experiments to be the most efficient working fluid for the U-tube ETC. However, no recent experiment has been done applying hybrid nanofluids in ETC, and since evidence already exists that

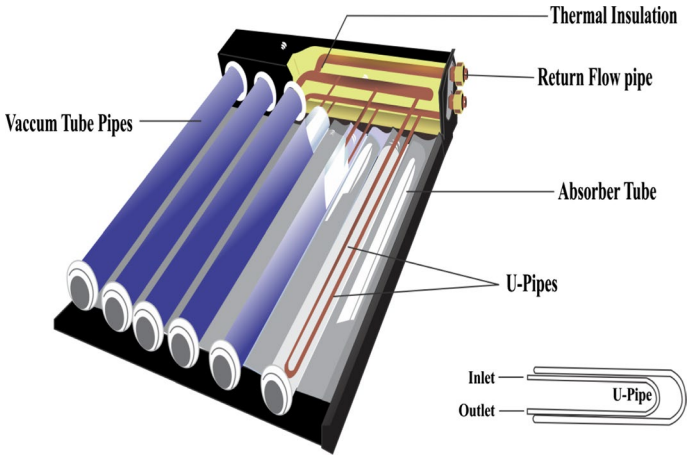

Fig. 10 Diagram of a U-tube collector cross section

hybrid nanofluids have better thermal performance than conventional nanofluids. It is the opinion of the authors that hybrid configuration of nanofluids may produce better performance than current efficiency provided by MWCNT nanofluid.

4.3 Nanofluids in Compound Parabolic Collectors

Lu et al. [180] carried out a novel experiment with an evacuated tubular solar collector with compound parabolic plates. The experiment assumed all solar irradiation from the CPC plate is transmitted into the glass tube, and the evacuated tube solar collector absorbed solar energy was transferred to the condenser. The experiment synthesized CuO–water nanofluids as the working fluid for this experiment. The nanofluid synthesized at mass concentrations of 0.8%, 1.0%, 1.2% and 1.5% with average particle size for the CuO NP at 50 nm. The experiment also considered filling ratios between 40% and 70% at intervals of 10. The optimum filling ratio for the evacuated tube was 60% as it presented the best evaporating heat transfer coefficient. The experiment also observed that 1.2% mass concentration provided optimal evaporating heat transfer coefficient and was 15% more efficient than deionized water under similar conditions. Liu et al. [181] further improved their earlier research by comparing the thermal performance of simple tubular CPC with truncated tubular CPC. The study observed that under similar conditions, working fluid temperatures in both simple tubular CPC and truncated tubular CPC were higher than an evacuated tube without CPC; also truncated tubular CPC had better thermal performance than simple CPC.

Investigations into the effects of nanofluids on CPC are not as much when compared to ETC and FPC. However, it is the opinion of the author that like in ETC and FPC the enhancements witnessed with the use of mono and hybrid nanofluids would be similar in the CPC as in the earlier discussed collectors.

4.4 Nanofluids in Solar Parabolic Trough Collector (PTC)

Several articles have investigated the use of nanoparticles dispersed in water for application in the PTC [182]. The performance of CuO water nanofluid and Al_2O_3 water nanofluid in a parabolic trough collector was theoretically investigated by Ghasemi and Ranjbar [183], using computational fluid dynamics (CFD). The study analyzed the effect of nanoparticle volume concentration on the thermal performance of the PTC. The result shows that when nanoparticle concentration was 3%, the heat transfer coefficient inside the receiver tube was enhanced by 28% for Al_2O_3 water nanofluid and 35% for CuO water nanofluid.

Subramani et al. [184] experimentally investigated the thermal efficiency and heat transfer performance of a PTC under turbulent flow, at varying volume concentrations of 0.05%, 0.1%, 0.2%, and 0.5% TiO_2 water nanofluid were compared with that of de-ionized water alone as a working fluid. The analysis was conducted under the turbulent flow regime ($2950 \leq Re \leq 8142$). Their result also showed at a volume concentration of 0.2%, the heat transfer coefficient enhancement, the thermal efficiency enhancement, and absorbed energy parameter was 22.75%, 8.66%, and 9.5% when compared to that of water. Importantly, the study developed correlations for the friction factor and Nusselt number.

Potenza et al. [185], performed an experimental study into the use of a parabolic trough collector with a transparent absorber tube using gas-phase nanofluid. The parabolic trough under evaluation employed 2-axis tracking to improve the efficiency of the readings. The transparent receiver was made with a coaxial tube and is vacuumed in its inner space. Air dispersed CuO nanopowder is used as a working fluid. The experiment was aimed at investigating the use of gas-based working fluid and a comparison of the experimental and numerical results was conducted. The authors observed the issue of deposition of nanopowder on the receiver pipe due to humidity. After 10 h of measurement in a day, they measured the working fluid

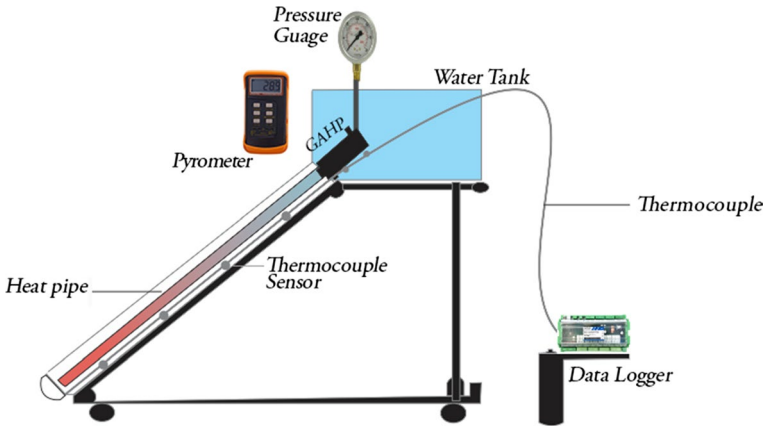

Fig. 11 Experiment outline diagram for nanofluid in the heat pipe system [165]

temperature greater than 145 °C with the maximum being 180 °C. The study measured a mean efficiency for the setup as 65%.

Coccia et al. [186] conducted a numerical evaluation of the yearly yield of a low enthalpy parabolic trough collector operating with six water-based nanofluids. The nanoparticles used are Fe_2O_3 (5,10,20 wt%), SiO_2 (1,5,25 wt%), TiO_2 (1, 10, 20, 35 wt.%), ZnO (1,5,10 wt%), Al_2O_3 (0.1, 1, 2 wt.%), Au (0.01 wt%). The effect of these nanoparticles on the thermal efficiency of the collector was investigated. Validation of their model was done with the result of two experimental setups located in Italy. The study considered different inlet temperatures to mass flow rate of 0.5 $kg{\cdot}min^{-1}$, 1 $kg{\cdot}s^{-1}$ and 1.5 $kg{\cdot}s^{-1}$. Their results show that the use of Al_2O_3, Au, TiO_2, ZnO, and nanofluids at small concentrations presented minimal improvements in thermal efficiency when compared to that of the water. The study highlighted that increasing the volume concentration of nanoparticle had no significant advantage when compared to water.

Okonkwo et al. [187] numerically compared the effect varied volume concentration of TiO_2 water nanofluid and SiO_2 water nanofluid had on the heat transfer coefficient. Results from the evaluation show that when the volumetric concentration was 3% the heat transfer coefficient of the collector was enhanced by 138% and 128% for SiO_2 water and TiO_2 water nanofluids, respectively. The authors observed that the use of the nanofluids led to a 14.85% drop in pressure but stated that the developed nanofluid presented a possible solution to the issue of cost, toxicity, and corrosion of component witnessed with conventional nanofluids.

Okonkwo et al. [188], conducted a study on the use of TiO_2–water nanofluids on a parabolic trough collector. A detailed entropy generation study on the performance of the collector was carried out and it was discovered that the use of the nanofluids decreased considerably the rate of entropy generation in the system especially at higher concentrations of nanoparticles, while also improving the thermal efficiency of the collector by 0.27%.

Nanofluids have also been applied to thermal oils commonly used in large scale parabolic trough installations. Mwesigye et al. [189] modeled Cu Therminol VP-1 nanofluid as the heat transfer fluid in the parabolic trough collector. The results from the study indicate that as volumetric concentration increased from 0% to 6%, the thermal efficiency of the PTC increases by 12.5%. The study states that the entropy generation rate in the collector is reduced by increasing the volume concentration of nanoparticle in the fluid.

Okonkwo et al. [190] performed a comparative study on the choice of working fluid to be used in a parabolic trough collector. The authors compared the use of pressurized water, supercritical carbon dioxide, Therminol VP-1, and 3 different oil-based nanofluids using CuO, Fe_3O_4, and Al_2O_3 nanoparticles, respectively. Their study showed that the use of the nanoparticles enhanced the performance of the thermal oil's properties of density, thermal conductivity, and viscosity while the specific heat capacity of the oil is reduced by using nanoparticles. The study also showed that using pressurized water gives a better thermal performance than all other working fluid considered. The hindrance to the use of pressurized water is the inability of the absorber to withstand high pressures. Their results showed that the use of Al_2O_3 Therminol VP-1 nanofluid provided the best improvement in thermal efficiency with

0.22% while CuO Therminol VP-1 and Fe_3O_4 Therminol VP-1 obtained enhancement of 0.18% and 0.15%, respectively.

Another study was performed from the synthesis of nanofluid from olive leaf extracts but using synthetic oil as the base fluid [191]. The authors obtained even better thermal performance with the use of syltherm-800 as the base fluid when compared to the use of water [187]. Thermal enhancement of 0.48% and 0.51% was observed with the use of OLE–TiO_2 oil and OLE–ZVI oil, respectively. The results, when compared to those found in literature, proved to be as reliable as those of conventional nanofluids.

Wang et al. [192] investigated the performance of a solar parabolic trough collector using Al_2O synthetic oil nanofluid as a heat transfer fluid; the experiment was carried out with a multi-field coupling simulation based on finite element method. Results show that the highest temperature of the absorber tube was reduced with the use of the Al_2O_3 synthetic oil. Also, as the volumetric concentration of nanoparticle was increased from 0% to 0.05% the deformation of the absorber caused by high operating temperature was decreased from 2.11 mm to 0.54 mm.

Bellos and Tzivanidis [193] numerically compared the effect of using Al_2O_3 syltherm-800 nanofluid, CuO syltherm-800 nanofluid, and syltherm-800 on the thermal efficiency of the parabolic trough collector. The result showed that both nanofluids had better thermal performance compare to syltherm-800. CuO syltherm-800 nanofluids showed the best thermal efficiency. Thermal efficiency was enhanced by 1.26% and 1.13% when heat transfer fluid was Al_2O_3 syltherm-800 nanofluid and CuO syltherm-800 nanofluid, respectively.

Using Al_2O_3 synthetic oil nanofluid under a turbulent regime with non-uniform heat flux, Sokhansefat et al. [194] evaluated the heat transfer performance of a PTC when operating temperatures were 300 K, 400 K, and 500 K. The effect of volume concentration on the thermal efficiency of the PTC was investigated and the result of the evaluation shows that the heat convection coefficient within the absorber tube was dependent on the volume concentration of nanoparticles in the fluid. Also, the heat transfer performance of the collector increased while the absorber temperature reduced.

Mwesigye et al. [195], also performed a thermodynamic evaluation on the performance of a PTC operating with Al_2O_3/synthetic oil as a working fluid. The study was performed while varying the Reynolds number from 3560 to 1,151,000 and for volumetric concentration ranging from 0 to 8%. The result of the study shows that the use of nanofluid improved the thermal efficiency of the collector by 7.6%. The optimal Reynolds number was also seen to decrease with an increase in the volumetric concentration.

So far, we have seen that the use of nanofluids impacts the thermal performance of the collector positively. Recently, as is the case with flat plate and evacuated tube collectors, the use of hybrid nanofluids has also gained research attention. Bellos and Tzivanidis [196], investigated the use of both conventional and hybrid nanofluids in a parabolic trough collector. The LS-2 module was studied comparing the thermal collector performance when syltherm-800, Al_2O_3/syltherm-800 nanofluid, TiO_2/syltherm-800 nanofluid, and Al_2O_3-TiO_2/syltherm-800 hybrid nanofluid. The volume concentration of the nanofluids was at 3%. The study was performed

under turbulent conditions with a flow rate of 150 $l \cdot min^{-1}$. The results of their study showed that the thermal efficiency enhancement of the hybrid nanofluid reached 1.8% while the use of mono nanofluid was 0.7%. They attributed the higher thermal efficiency enhancement to the greater Nusselt number enhancement witnessed with the use of the hybrid nanofluid.

Minea [197], performed a numerical evaluation of hybrid nanofluids based on Al_2O_3, TiO_2, and SiO_2. They stated that the heat transfer behavior of the nanofluids was dependent on their thermophysical properties. Citing that the thermal properties of all the nanofluid increased with the addition of more nanoparticle with the thermal conductivity enhancement increased by at least 12%. The author also developed a new correlation for obtaining the Nusselt number of alumina nanofluid along with its hybrids.

Minea and El-Maghlany [198], performed a study on the influence of hybrid nanofluid on the performance of a parabolic trough collector. They stated that the use of ordinary heat transfer fluids is limited due to their thermal conductivity, the use of nanofluid and later hybrid nanofluids provides an opportunity for increasing the performance of these working fluids. The authors demonstrated an enhancement in the Nusselt number for all hybrid nanofluids. The use of Cu–Mgo hybrid nanofluid at a 2% volumetric concentration, provided a 14% increase in the values of Nusselt number when compared to that of the base fluid. They also highlighted that the use of the hybrid nanofluid produced increased viscosity in the fluid which leads to pressure drop. The use of 2% Ag-MgO water increases the collector efficiency and Reynolds number in the system. The authors highlighted the need for more experimental and numerical works to implement the use of new heat transfer fluids in solar collectors.

Results of many of the surveyed literature favor the use of the nanofluids in the solar collectors as it improves the thermal performance of the collector. This is done by increasing the thermal conductivity of the fluid and reducing the thermal boundary layer. The application of these nanofluids, however, has suffered many limitations such as sedimentation of particles in the absorber, corrosion of components, the high cost of preparation of the nanofluid, the toxicity of the nanoparticles, their parasitic effect on pressure drop and the requirement for additional pump power [199]. These limitations have hindered the deployment of nanofluids as heat transfer fluids in solar collectors.

From Table 6, it can be inferred that the thermal efficiency of parabolic through collectors are improved by nanofluids when compared to the regular heat transfer fluids. Like in non-concentrating collectors increase in volume concentration increases the thermal performance of the PTC. Further research is required to fully understand the effects of hybrid nanofluids within the PTC.

Like in the non-concentrating systems, nanofluids made up of carbon material is among the best performing nanofluids. It is the opinion of the authors, almost without a doubt the optimum nanofluid material for heat transfer application will contain carbon within its configuration.

Table 5 Studies of nanofluids in evacuated tube solar collectors

Author	Base fluid	Preparation method	NP	Particle size (nm)	Dispersant	Volume concentration (%)	Evacuated tube type	Mass flow rate ($kg \cdot min^{-1}$>)	Absorption area (m^2)	Result highlights/remarks
Pise et al. 2015 [162]	Water	Two-step	Al_2O_3	50	Not available	0.05%, 0.1%, 0.5%	Heat Pipe	0.2	0.288	Collector efficiency increased with an increase in tilt angle from 18.63 to 50 degrees. However, it reduces with a further increase in the collector tilt angle. Collector efficiency increased with an increase in volume concentration for the considered range. The maximum efficiency improvement compared to water was 15.24%

Table 5 (continued)

Author	Base fluid	Preparation method	NP	Particle size (nm)	Dispersant	Volume concentration (%)	Evacuated tube type	Mass flow rate ($kg \cdot min^{-1}$>)	Absorption area (m^2)	Result highlights/remarks
Kim et al. 2017 [163]	Distilled water	Two-step	Al_2O_3	20, 50, 100	Not applicable	0.5%, 0.1%,1.5%	U-Tube	1.98, 2.82	2.37	Thermal conductivity in nanofluid rises with an increase in volume concentration between 0% and 1%, however, it decreases between 1% and 1.5%. The maximum collector efficiency improvement was 24.1% as compared to water under the same conditions

Table 5 (continued)

Author	Base fluid	Preparation method	NP	Particle size (nm)	Dispersant	Volume concentration (%)	Evacuated tube type	Mass flow rate ($kg \cdot min^{-1}$>)	Absorption area (m^2)	Result highlights/remarks
Ghaderian and Sidik 2017 [164]	Distilled water	Two-step	Al_2O_3	40	Not applicable	0.03%, 0.06%	ETSC	0.33, 0.67, 1	2.36	Collector efficiency increased with an increase in mass flow rate and volume concentration within the considered range. Maximum collector efficiency at 0.03% and 0.06% volume concentration was 39.52% and 58.65%, respectively, while water under similar conditions was 22.85%

Table 5 (continued)

Author	Base fluid	Preparation method	NP	Particle size (nm)	Dispersant	Volume concentration (%)	Evacuated tube type	Mass flow rate ($kg \cdot min^{-1}$>)	Absorption area (m^2)	Result highlights/remarks
W. Kang, Shin, and Cho 2019 [32]	Water	two-step	CuO	40, 80	Arabic gum	0.1%, 0.3%, 0.5%, 0.7%	U-Tube	–	2.37	Collector efficiency rises with an increase in volume concentration between 0% and 0.5%, however, it decreases between 0.5% and 0.7%. The maximum efficiency improvement is 7.2% as compared to water under similar conditions

Table 5 (continued)

Author	Base fluid	Preparation method	NP	Particle size (nm)	Dispersant	Volume concentration (%)	Evacuated tube type	Mass flow rate ($kg \cdot min^{-1}$>)	Absorption area (m^2)	Result highlights/remarks
Eidan et al. 2018 [165]	Acetone	Two-step	Al_2O_3, CuO	20, 25	Not applicable	0.25%, 0.5%	Heat pipe	0.0, 0.02,0.03	0.06912	Nanofluids were used as working fluid within the heat pipe. optimal filling ratio, tilt angle, and volume concentration was 70%, 30-degree, and 0.5%. Thermal performance increase with a reduction in nanoparticle size
Mahendran et al. 2013 [169]	Water	Two-step	TiO_2	40	Not applicable	1%, 2%, 3%	U-tube	1, 2,3	3.7	Increase in mass flow rate improves thermal efficiency and reduces entropy generation

Table 5 (continued)

Author	Base fluid	Preparation method	NP	Particle size (nm)	Dispersant	Volume concentration (%)	Evacuated tube type	Mass flow rate ($kg \cdot min^{-1}$>)	Absorption area (m^2)	Result highlights/remarks
Gan et al. 2018 [167]	Distilled water	Two-step	TiO_2	21	PVP	0.1%,0.3%, 0.5%	Heat pipe	1.02, 1.5, 1.98	1.92	Using the optimal volume concentration, surfactant ratio and sonication time was 0.5%, 1:1, and 10 min. An increase in sonication time does not have any major effect on the thermal properties of the liquid

Table 5 (continued)

Author	Base fluid	Preparation method	NP	Particle size (nm)	Dispersant	Volume concentration (%)	Evacuated tube type	Mass flow rate ($kg \cdot min^{-1}$>)	Absorption area (m^2)	Result highlights/remarks
M. A. Sharafeldin and Gróf 2018a [170]	Water	Two-step	CeO_2	25	Not applicable	0.015, 0.025, 0.035	Heat pipe	0.78, 0.9, 1.02	1.59	Thermal efficiency improved with an increase in concentration with the considered range. The maximum efficiency improvement was 37.3% compared to water under similar conditions

Table 5 (continued)

Author	Base fluid	Preparation method	NP	Particle size (nm)	Dispersant	Volume concentration (%)	Evacuated tube type	Mass flow rate ($kg \cdot min^{-1}$>)	Absorption area (m^2)	Result highlights/remarks
M. A. Sharafeldin and Gróf 2019 [171]	Water	Two-step	WO_3	90	Not applicable	0.014, 0.028, 0.042	Heat pipe	0.78, 0.9, 1.02	1.59	Thermal efficiency improved with an increase in concentration with the considered range. Maximum efficiency improvement was 19.3% better compared to water under similar working

Table 5 (continued)

Author	Base fluid	Preparation method	NP	Particle size (nm)	Dispersant	Volume concentration (%)	Evacuated tube type	Mass flow rate ($kg \cdot min^{-1}$>)	Absorption area (m^2)	Result highlights/remarks
Kaya, Arslan, and Eltugral 2018 [172]	Ethylene glycol–pure water	Two-step	ZnO	30	Not applicable	1%, 2%, 3%, 4%	U-tube	1.2, 1.8, 2.7	2.3	Collector efficiency improved with an increase in volume concentration from 1% to 3% but reduced as volume concentration increased between 3 and 4%. Maximum collector efficiency enhancement was obtained as 62.87%

Table 5 (continued)

Author	Base fluid	Preparation method	NP	Particle size (nm)	Dispersant	Volume concentration (%)	Evacuated tube type	Mass flow rate ($kg \cdot min^{-1}$>)	Absorption area (m^2)	Result highlights/remarks
Yan et al. 2017 [173]	Distilled water	Two-step	SiO_2	30	Not applicable	1%, 3%, 5%	ETSC	Not applicable	0.1	Transmissivity improved with a reduction in volume concentration. The viscosity of working fluid increased with increase in volume concentration

Table 5 (continued)

Author	Base fluid	Preparation method	NP	Particle size (nm)	Dispersant	Volume concentration (%)	Evacuated tube type	Mass flow rate ($kg \cdot min^{-1}$>)	Absorption area (m^2)	Result highlights/remarks
Ozsoy and Corumlu 2018 [174]	Water	One-step chemical	Ag	40	Not applicable	0.001	Heat pipe	0.18	0.22	Nanofluids were used within working fluid within the heat pipe. Nanofluid absorption dropped by approximately 52% after one year. Thermal conductivity of Ag–water nanofluid is directly depended on the temperature change

Table 5 (continued)

Author	Base fluid	Preparation method	NP	Particle size (nm)	Dispersant	Volume concentration (%)	Evacuated tube type	Mass flow rate ($kg \cdot min^{-1}$>)	Absorption area (m^2)	Result highlights/remarks
Hussain, Jawad, and Sultan 2015 [176]	Distilled water	Two-step	Ag, ZrO_2	30 nm 50 nm	Not applicable	1%, 3%, 5%	ETSC	0.5, 1, 1.5	Not Available from text	solar collector efficiency using Ag–water nanofluid was greater than ZrO2/water nanofluid under similar condition
Mahbubul et al. 2018 [177]	Distilled water	Two-step	SWCNT	I = 2 µm, d = NA	Not applicable	0.05, 0.1, 0.2	ETSC	NA	42	Maximum efficiency improvement of 10%

5 Economic Analysis of Nanofluids in Collectors

The efficiency of solar collectors is a ratio of the useful energy gained by the collectors to the total energy supplied by the sun. The economic utility of nanofluid within a collector is assessed by either calculating the overall reduction in the size of the collectors [211] or by calculating the environmental cost implication of energy generation from solar collectors and comparing it to generating the same amount of energy with conventional energy sources [212]. While under high irradiance condition FPCs are more efficient than ETCs under poor irradiance the ETC tends to outperform the FPC [210]. Significant investigations to understand the economic viability of collector systems with nanofluids as heat transfer fluids have been performed by researchers. In an experiment conducted by Stalin et al. [211], it was observed that CeO2 water nanofluid could reduce the overall size of the FPC by as much as 26%. Also, Faizal et al. [130] calculated that the simple payback period for applying SiO2 nanofluid within a flat plate collector is about two (2) months. Kang et al. [212] calculated that it was possible to annually offset CO2 emissions by 83.04 kg and SO2 emissions by 0.7 kg when Al2O3 nanofluid is applied in FPC. When the same nanofluid was applied in ETC it was possible to offset CO2 emissions by 473.65 kg and SO2 emissions by 01.33 kg.

6 Limitations of Nanofluids in Collectors

There are several advantages of employing nanofluids in solar thermal collectors. These advantages include an increase in thermal efficiency, a possible reduction in collector size, and improved economic and environmental performance. However, there are still several limitations in the performance and predictability of nanofluids in collectors.

One of the limiting factors in the application of nanofluids in solar collectors is the stability of nanofluid. Unlike conventional working fluids, nanofluids are highly unstable and particles tend to sediment after some time. As nanoparticles continue in Brownian motion within the fluid, they are attracted to each other. While pH modulation, preparation technique, and surfactant addition may reduce agglomeration within the fluid. The overall efficiencies of collector systems still drastically reduce over extended periods because of the reduction in fluid stability. As observed by Bulut and Özacar [175], absorbance in nanofluid decreased by 52% after one year; this drop is far more significant than the efficiency improvement provided by the nanofluid. Also, continuous aggregation increases the fluid viscosity, which will reduce the flow rate in thermosyphons or increase the pump power required in forced convection systems. Both of which will ultimately reduce the system's efficiency. While the thermal performance of nanofluid is superior to conventional heat transfer fluid in many heat transfer systems, in evaporative systems like heat pipes, some limitations still exist. The evaporation in heat pipes leads to increased aggregation within the fluid, which then lowers the evaporation rates [216].

The hysteresis phenomenon first observed by Nguyen et al. [217] poses another significant limitation in the application of nanofluids in solar collectors, especially in concentrating systems. The apparent damage in the nanofluids rheology observed when nanofluids are heated beyond the critical temperature negatively affects their applicative properties. Since concentrating collectors operate at high temperatures, and the inability of nanofluids to return to their heating viscosities when cooled poses an engineering challenge to their application. It is important to note that this phenomenon has been observed in several different nanofluids at temperatures between 60 – 70 °C for water-based nanofluids.

While it is of significant benefit to heat transfer applications that nanofluids have much higher Nusselt numbers compared to conventional fluids. The inability to generally predict the Nusselt number value of nanofluids limits the direct application of the fluids. From the heat transfer correlation studies conducted for different nanofluids [74, 218, 219], it appears that the value of the Nusselt number is completely dependent on the configuration of the nanofluid. Since nanofluids can be configured by size, shape, material, concentration, etc., there is almost an infinite number of configurations for nanofluids. Many Nusselt number correlations are required to predict the heat transfer performance of the different nanofluids. Also, very little is known on the effect of hysteresis on the long-term heat transfer performance of nanofluids since the fluid viscosity plays a significant rule in heat transfer.

Till now questions still exists with the numerical prediction of the rheological properties of nanofluids. Answers to these questions would unlock the potential of nanofluids in several applications. Many researchers are continually trying to predict these thermal and rheological properties of nanofluids; however, these studies have been held back by the apparent infinite active variables that appear to dictate the rheology of nanofluids. These "active variables" include volume concentration, base fluid, nanoparticle size, packing fraction, nanolayers, particle distribution, agglomeration, pH, and temperature. The extensive nature of these active variables makes it difficult for researchers to predict the thermal and rheological properties of nanofluids accurately.

While there are some known facts about the relationship between the active variables and the nanofluid thermophysical properties, like an increase in particle volume concentration leads to an increase in thermal conductivity and viscosity. It is essential to point out that some relationships between these active variables and the nanofluid's thermophysical properties are not clear. For instance, the relationship between particle size and viscosity remains uncovered as some studies claim viscosity increases with an increase in particle size while others claim viscosity reduces with an increase in particle size [220]. These questions that surround the number of active variables that affect the thermophysical properties, and the extent to which these variables affect the nanofluid properties, must be completely answered before we can have accurate nanofluid behavior models.

In viscosity prediction, researchers have proposed several formulas. Many of which modify existing equations accounting for previous unconsidered variables. Einstein's work provided the premier understanding of colloidal dispersions, as seen in Eq. 27. Einstein's work was modified to account for the effect of volume concentration [114], the cumulative work of Einstein, Krieger, and Dougherty was

modified to account for packing fraction [221]. Successively, there have been additional modifications to account for other unaccounted variables. However, none of these proposed models has provided accurate predictions or constant deviations when compared with experimental observations.

These same limitations apply when predicting the thermal conductivity of nanofluids. Maxwell provided researchers with a fundamental understanding of the basic properties [46]. Yu and Choi modified Maxwell's equation to account for interfacial layers [89]. Further modifications were performed to account for particle aggregation [222]. Also, all these proposed models are yet to accurately predict the thermal conductivity of nanofluids. To improve on these limitations, further experiments are necessary with emphasis on the effect of the active variables on the rheological properties of nanofluids.

Another limitation exists in the numerical modeling of nanofluids as heat transfer fluids in collectors. Collector flow models are dependent on the thermophysical properties of the heat transfer fluid. Therefore, any inaccuracies in the nanofluid thermophysical property model would lead to inaccuracies in modeling the flow and heat transfer within the collector.

7 Conclusion

This study presents a review of the applications of nanofluids in four different solar thermal collectors. Several studies have determined the influence of nanofluids as heat transfer fluids in flat plate collectors, evacuated tube collectors, and parabolic trough collectors, However, studies to determine the effects of nanofluids in compound parabolic collectors and other concentrating collectors are very few. From the literature reviewed in this study, the authors make these concluding remarks:

- Nanofluids as working fluids improve the thermal performance of collectors compared to conventional working fluids. This improvement is mainly due to the improved thermal conductivity of nanofluids.
- Most researchers synthesize nanofluids by the two-step method; this is due to the relative ease of this method of synthesis and the ability to control the volume concentration of the nanofluids. However, the one-step synthesis technique presents more stable nanofluids for heat transfer applications.
- Artificial neural network models are the closest models for predicting the thermo-physical behavior of nanofluids. The accuracy of these models will further improve with an increase in available experimental data.
- An increase in volume concentration increases the thermal conductivity of the nanofluid, which ultimately improves the collector efficiency. However, multiple studies for both flat plate and evacuated tube collectors have observed that there exists an optimum point where further increase in volume concentration will not increase the thermal efficiency performance of the collector. This optimum exists because an increase in volume concentration leads to an increase in fluid viscosity.

Table 6 Some studies that evaluated the thermal performance observed with the use of nanofluids in the PTC

Literature study	Nanofluids	Methodology	Nanoparticle volumetric concentration	Thermal efficiency or enhancement observed
Bellos and Tzivandis [196]	Al_2O_3/oil	Numerical study	3 vol %	0.34%
	TiO_2/oil		3 vol %	0.34%
Mwesigye et al. [195]	Al_2O_3/oil	CFD analysis	8 vol %	7.6%
Bilal et al. [200]	Fe_3O_4/water	Numerical study	0.6 vol %	1.6%
Hatami et al. [201]	Cu, TiO_2, Al_2O_3, Fe3O4/water	CFD analysis	8 vol %	–
Mwesigye et al. [43]	Cu, Ag, Al_2O_3/oil	CFD analysis	6 vol %	13.9%
Mwesigye et al. [202]	SWCNT/oil	CFD analysis	2.5 vol %	4.4%
Okonkwo et al. [188]	TiO_2/water	Numerical study	3 vol %	0.27%
Okonkwo et al. [203]	Al_2O_3/oil	Numerical study	3 vol %	0.73%
Bellos and Tzivandis [193]	Al_2O_3/oil	Numerical study	4 vol %	1.13%
	CuO/oil		4 vol %	1.26%
Subramani et al. [184]	TiO_2/water	Experimental study	2 vol %	8.6%
Subramani et al. [204]	Al_2O_3/water	Experimental study	0.05–0.5 vol %	8.54%
Okonkwo et al. [190]	Al2O3, CuO, Fe3O4/oil	Numerical study	3 vol %	0.22%
Kasaeian et al. [205]	MWCNT/mineral oil	Experimental study	0.3 vol %	7%
Menbari et al. [206]	CuO/water	Experimental study	0.008 vol %	52%
Chaudhari et al. [207]	Al_2O_3/water	Experimental study	0.1 vol %	7%
Basbous et al. [208]	Al_2O_3/oil	Numerical study	5 vol %	–
Bellos et al. [209]	Al_2O_3/oil	CFD analysis	2 vol %	4.25%
Wang et al. [192]	Al_2O_3/oil	CFD analysis	5 vol %	1.2%
Kaloudis et al. [210]	Al_2O_3/oil	CFD analysis	4 vol %	–
Mwesigye et al. [211]	Al_2O_3/water	CFD analysis	6 vol %	–
Kasaeian et al. [212]	MWCNT, SiO_2/EG water	Experimental study	0.3 vol %	30.4%
Khullar et al. [213]	Al_2O_3/oil	Numerical study	0.05 vol %	5–10%

Table 6 (continued)

Literature study	Nanofluids	Methodology	Nanoparticle volumetric concentration	Thermal efficiency or enhancement observed
Nayak et al. [214]	Al_2O_3/oil	Numerical study	5 vol %	–
Allouhi et al. [215]	CuO/oil	Numerical study	5 vol %	~0%
Ghasemi and Ranjbar [183]	Al_2O_3/water	CFD analysis	3 vol %	–
	CuO/water		3 vol %	–
Okonkwo et al. [187]	OLE–TiO_2/water	Experimental study	3 vol %	0.077%
	BH–SiO_2/water		3 vol %	0.073%
Okonkwo et al. [191]	OLE–TiO_2/oil	Experimental study	3 vol %	0.48%
	OLE–ZVI/oil		3 vol %	0.51%

- Collector efficiency is lower when viscosity in nanofluids is high and vice versa. This phenomenon is noticed in both thermosyphon and force convection systems. In thermosyphon, the efficiency is reduced because of the reduction in flow rate at high viscosity while in forced convection, the pumping power is increased.
- A rise in flow rate leads to an increase in collector efficiency. However, there exists an optimum flow rate where any further increase in flow rate does not raise the thermal efficiency of the collector system.
- Conventional nanofluids with carbon allotropes dispersed in them have shown better, thermal absorption and efficiency enhancements compared to metal and metal oxide nanofluids. Among the conventional metal oxides, CuO is observed to have the best thermal absorption properties.
- Stable nanofluids improve the efficiency of collectors, especially over long periods. The synthesis techniques used, dispersant addition and pH modulation present ways of improving the stability of nanofluids.
- Nanofluids in heat pipes have improved the evaporating heat transfer coefficient compared to the conventional fluids. However, constant evaporation and condensation negatively affect the long-term stability of the nanofluids.
- In collectors with heat pipes, increasing the filling ratio of the heat pipe increases the heat transfer coefficient. However, an optimum filling ratio exists where a further increase in filling does not increase heat transfer in the condensation area. This optimum filling ratio is usually between 60% and 70% depending on the tilt angle (angle of inclination).
- Studies have shown that hybrid nanofluids improve the thermal efficiency of collectors compared to conventional nanofluids in solar thermal collectors. However, there have been very few hybrid studies for compound parabolic collectors, heat pipes, and most concentrating collectors.

Funding Open Access funding provided by the Qatar National Library.

Compliance with Ethical Standards

Conflict of interest The authors also would like to state that there exists no conflict of interest either financially or through other personal considerations that may compromise or have the appearance of compromising the authors' professional judgment in conducting or reporting this study.

References

1. E. Dupont, R. Koppelaar, H. Jeanmart, (2020) Global available solar energy under physical and energy return on investment constraints. Appl. Energy **257**, 113968 (2020)
2. S. Hoseinzadeh, R. Azadi, Simulation and optimization of a solar-assisted heating and cooling system for a house in Northern of Iran. J. Renew. Sustain. Energy **9**, 045101 (2017)
3. O.O. Bamisile, A.A. Babatunde, M. Dagbasi, I. Wole-Osho, Assessment of solar water heating in Cyprus: utility, development and policy. Int. J. Renew. Energy Res. **7**, 448–1453 (2017)
4. S. Hoseinzadeh, R. Ghasemiasl, M. A. Javadi, P. S. Heyns, Performance evaluation and economic assessment of a gas power plant with solar and desalination integrated systems. (2020)
5. S. Hoseinzadeh, M. Hadi Zakeri, A. Shirkhani, A.J. Chamkha, Analysis of energy consumption improvements of a zero-energy building in a humid mountainous area. J. Renew. Sustain. Energy **11**, 015103 (2019)
6. R. Ghasemiasl, S. Hoseinzadeh, M.A. Javadi, Numerical analysis of energy storage systems using two phase-change materials with nanoparticles. J. Thermophys. Heat Transf. **32**, 440–448 (2018)
7. S. Kalogirou, *Solar Energy Engineering*. (2009)
8. S.U.S. Choi, J.A. Eastman, Enhancing thermal conductivity of fluids with nanoparticles. *Am*. Soc. Mech. Eng. Fluids Eng. Div. FED **231**, 99–105 (1995)
9. H.W. Xian, N.A.C. Sidik, G. Najafi, Recent state of nanofluid in automobile cooling systems. J. Therm. Anal. Calorim. **135**, 981–1008 (2019)
10. M.U. Sajid, H.M. Ali, Recent advances in application of nanofluids in heat transfer devices : A critical review. Renew. Sustain. Energy Rev. **103**, 556–592 (2019)
11. S. Thomas, C.B. Panicker Sobhan, A review of experimental investigations on thermal phenomena in nanofluids. Nanoscale Res. Lett. **6**, 377 (2011)
12. S.A. Kalogirou, Solar thermal collectors and applications. Prog. Energy Combust. Sci. **30**, 231–295 (2004)
13. J. Qin, E. Hu, G.J. Nathan, L. Chen, Concentrating or non-concentrating solar collectors for solar Aided Power Generation? *Energy Convers*. Manag. **152**, 281–90 (2017)
14. S. Hess, *Solar Thermal Process Heat (SPH) Generation, in Renewable Heating and Cooling: Technologies and Applications* (Woodhead Publishing, New York, 2015)
15. M. Eltaweel, A.A. Abdel-Rehim, Energy and exergy analysis of a thermosiphon and forced-circulation flat-plate solar collector using MWCNT/Water nanofluid. Case Stud. Therm. Eng. **14**, 100416 (2019)
16. H.C. Hottel, B.B. Woertz, The performance of flat-plate solar-heat collectors. Trans. ASME **64**, 91–104 (1942)
17. E. Özil, K. Yaşar, Analysis of flat plate collectors, *solar energy utilization* (Springer, Dordrecht, 1987), pp. 188–213
18. M. Khamis Mansour, Thermal analysis of novel minichannel-based solar flat-plate collector. Energy **60**, 333–343 (2013)
19. Y. Deng, Y. Zhao, W. Wang, Z. Quan, L. Wang, D. Yu, Experimental investigation of performance for the novel flat plate solar collector with micro-channel heat pipe array (MHPA-FPC). Appl. Therm. Eng. **54**, 440–449 (2013)
20. S. Föste, A. Pazidis, R. Reineke-Koch, B. Hafner, D. Mercs, C. Delord, Flat Plate Collectors with Thermochromic Absorber Coatings to Reduce Loads during Stagnation. Energy Procedia **91**, 42–48 (2016)
21. J. Jyothi, H. Chaliyawala, G. Srinivas, H.S. Nagaraja, H.C. Barshilia, Design and fabrication of spectrally selective TiAlC/TiAlCN/TiAlSiCN/TiAlSiCO/TiAlSiO tandem absorber for higherature solar thermal power applications. Sol. Energy Mater. Sol. Cells **140**, 209–216 (2015)
22. H.C. Barshilia, N. Selvakumar, K.S. Rajam, Thermal stability of TiAlN/TiAlON/Si3N4 tandem absorbers prepared by reactive direct current magnetron sputtering. *J. Vac. Sci*. Technol. A Vacuum, Surfaces, Film. **516**, 6071–6078 (2007)
23. R. Bakari, R. J. A. Minja, K. N. Njau, Effect of glass thickness on performance of flat plate solar collectors for fruits drying. *J. Energy*. (2014)
24. N. Ehrmann, R. Reineke-Koch, S. Föste, F. Giovannetti, The influence of process parameters and coating properties of double glazing coated with transparent conducting oxides on the efficiency of solar-thermal flat-plate collectors. Thin Solid Films **532**, 132–140 (2013)

25. P.V. Ranjith, A.A. Karim, A comparative study on the experimental and computational analysis of solar flat plate collector using an alternate working fluid. Procedia Technol. **24**, 546–553 (2016)
26. E.C. Okonkwo, I. Wole-osho, D. Kavaz, M. Abid, T. Al-ansari, (2020) Thermodynamic evaluation and optimization of a flat plate collector operating with alumina and iron mono and hybrid nanofluids. Sustain. Energy Technol. Assessments **37**, 100636 (2020)
27. S. Kalogirou, The potential of solar industrial process heat applications. Appl. Energy **76**(4), 337–361 (2003)
28. L.M. Ayompe, A. Duffy, M. Mc Keever, M. Conlon, S.J. McCormack, Comparative field performance study of flat plate and heat pipe evacuated tube collectors (ETCs) for domestic water heating systems in a temperate climate. Energy. **36**, 3370–8 (2011)
29. G.L. Morrison, I. Budihardjo, M. Behnia, Water-in-glass evacuated tube solar water heaters. Sol. Energy. **76**, 135–40 (2004)
30. G.L. Morrison, N.H. Tran, D.R. McKenzie, I.C. Onley, G.L. Harding, R.E. Collins, Long term performance of evacuated tubular solar water heaters in Sydney, Australia. Sol. Energy **32**, 785–791 (1984)
31. M. Hayek, J. Assaf, W. Lteif, Experimental investigation of the performance of evacuated-tube solar collectors under eastern mediterranean climatic conditions. Energy Procedia **6**, 618–626 (2011)
32. W. Kang, Y. Shin, H. Cho, Experimental investigation on the heat transfer performance of evacuated tube solar collector using CuO nanofluid and water. J. Mech. Sci. Technol. **33**(3), 1477–1485 (2019)
33. R. Winston, Principles of solar concentrators of a novel design. Sol. Energy **16**, 89–95 (1974)
34. A. Rabl, *Active Solar Collectors and Their Applications*. (1985)
35. R. Tchinda, N. Ngos, A theoretical evaluation of the thermal performance of CPC with flat one-sided absorber. Int. Commun. Heat Mass Transf. **33**(6), 709–718 (2006)
36. J.M. Gordon, Nonimaging Solar Energy Concentrators (CPC's) with fully illuminated flat receivers: a viable alternative to flat-plate collectors. J. Sol. Energy Eng. **108**(3), 252 (2010)
37. H.P. Baum, J.M. Gordon, *Optimal design of nonimaging solar concentrators with wedge receivers* (Appl, Opt, 2009)
38. A. Rabl, J. O'Gallagher, R. Winston, Design and test of non-evacuated solar collectors with compound parabolic concentrators. Sol. Energy **25**(4), 335–351 (1980)
39. J.A. Duffie, W.A. Beckman, *Solar engineering of thermal processes solar engineering* (Wiley, New York, 2013)
40. E.C. Okonkwo, H. Adun, A.A. Babatunde, M. Abid, T.A.H. Ratlamwala, Entropy generation minimization in a parabolic trough collector operating with SiO 2 - water nanofluids using genetic algorithm and artificial neural network. J. Therm. Sci. Eng. Appl. **12**, 031007 (2020)
41. E.C. Okonkwo, T.A.H. Ratlamwala, M. Abid, Energy, exergy, exergoeconomic, and exergoenvironmental study of a parabolic trough collector using a converging-diverging receiver tube. Int. J. Exergy **29**, 131–154 (2019)
42. E.C. Okonkwo, M. Abid, T.A.H. Ratlamwala, Comparative study of heat transfer enhancement in parabolic trough collector based on modified absorber geometry. J. Energy Eng. **145**(3), 04019007 (2019)
43. A. Mwesigye, J.P. Meyer, Optimal thermal and thermodynamic performance of a solar parabolic trough receiver with different nanofluids and at different concentration ratios. Appl. Energy **193**, 393–413 (2017)
44. S. Choi, J. A. Eastman, Enhancing thermal conductivity of fluids with nanoparticles. *No. ANL/MSD/CP-84938; CONF-951135–29*, (Argonne National Lab., IL (United States)), (1995)
45. E.C. Okonkwo, I. Wole-Osho, I.W. Almanassra, Y.M. Abdullatif, T. Al-Ansari, An updated review of nanofluids in various heat transfer devices. J. Therm. Anal. Calorim. **15**, 1–56 (2020)
46. J.C. Maxwell, *A Treatise on Electricity and Magnetism [Volume 2]* (Clarendon Press, London, 1881)
47. S.M. Peyghambarzadeh, S.H. Hashemabadi, M.S. Jamnani, S.M. Hoseini, Improving the cooling performance of automobile radiator with Al 2O3/water nanofluid. Appl. Therm. Eng. **31**, 1833–8 (2011)
48. E.C. Okonkwo, I. Wole-Osho, D. Kavaz, M. Abid, Comparison of experimental and theoretical methods of obtaining the thermal properties of alumina/iron mono and hybrid nanofluids. J. Mol. Liq. **292**, 111377 (2019)

49. R. Manimaran, K. Palaniradja, N. Alagumurthi, S. Sendhilnathan, J. Hussain, Preparation and characterization of copper oxide nanofluid for heat transfer applications. Appl. Nanosci. **4**, 163–167 (2014)
50. M.G. Guzmán, J. Dille, S. Godet, Synthesis of silver nanoparticles by chemical reduction method and their antibacterial activity. Int. J. Chem. Biomol. Eng. **2**, 104–11 (2009)
51. C. Pinto, R.J. Neufeld, A.J. Ribeiro, F. Veiga, Nanoencapsulation I Methods for preparation of drug-loaded polymeric nanoparticles. Nanomed. Nanotechnol. **2**(1), 8–21 (2006)
52. A. Asadi, I.M. Alarifi, V. Ali, H.M. Nguyen, An experimental investigation on the effects of ultrasonication time on stability and thermal conductivity of MWCNT-water nanofluid: Finding the optimum ultrasonication time. Ultrason. Sonochem. **58**(April), 104639 (2019)
53. I.W. Almanassra, A.D. Manasrah, U.A. Al-Mubaiyedh, T. Al-Ansari, Z.O. Malaibari, M.A. Atieh, An experimental study on stability and thermal conductivity of water/CNTs nanofluids using different surfactants: A comparison study. J. Mol. Liq. **304**, 111025 (2019)
54. W. Chen, C. Zou, X. Li, Application of large-scale prepared MWCNTs nanofluids in solar energy system as volumetric solar absorber. Sol. Energy Mater. Sol. Cells **200**, 109931 (2019)
55. N.A. Bin-Abdun, Z.M. Razlan, S.A. Bakar, C.H. Voon, Z. Ibrahim, W.K. Wan, M.J.M. Ridzuan, Heat transfer improvement in simulated small battery compartment using metal oxide (CuO)/deionized water nanofluid. Heat Mass Transf. und Stoffuebertragung. **56**, 399–406 (2019)
56. A. Abadeh, M. Passandideh-Fard, M.J. Maghrebi, M. Mohammadi, Stability and magnetization of Fe 3 O 4 /water nanofluid preparation characteristics using Taguchi method. J. Therm. Anal. Calorim. **135**(2), 1323–1334 (2019)
57. T. Rajendra Prasad, K. Rama Krishna, K.V. Sharma, Experimental testing of thermo physical properties of novel water and glycerol mixture-based silica nano fluids. Int. J. Recent Technol. Eng. **8**(2), 5299–5305 (2019)
58. N.S. Binti Rukman, A. Fudholi, N.F. Mohd Razali, M. Hafidz Ruslan, K. Sopian, Investigation of TiO2 and MWCNT Nanofluids-based Photovoltaic-Thermal (PV/T) System. IOP Conf. Ser. Earth Environ. Sci. **268**, 1 (2019)
59. D.P. Barai, B.A. Bhanvase, V.K. Saharan, Reduced Graphene Oxide-Fe_3O_4 nanocomposite based nanofluids: study on ultrasonic assisted synthesis, thermal conductivity, rheology, and convective heat transfer. Ind. Eng. Chem. Res. **58**, 8349–8369 (2019)
60. A. Afzal, S.A. Khan, C. Ahamed Saleel, Role of ultrasonication duration and surfactant on characteristics of ZnO and CuO nanofluids. Mater. Res. Express **6**, 11 (2019)
61. J.A. Eastman, S.U.S. Choi, S. Li, W. Yu, L.J. Thompson, Anomalously increased effective thermal conductivities of ethylene glycol-based nanofluids containing copper nanoparticles. Appl. Phys. Lett. **78**, 718–720 (2001)
62. S. Lin, Y. Chen, X. Tan, F. Song, E.Y.B. Pun, Z. He, J. Pu, Catalytic performance of Fe 3 O 4 nanoparticles for cyclocondensation synthesis of thiacrown ethers. Mater. Res. Express **2**, 015010 (2015)
63. H.T. Zhu, C.Y. Zhang, Y.M. Tang, J.X. Wang, Novel synthesis and thermal conductivity of CuO nanofluid. J. Phys. Chem. C. **111**, 1646–50 (2007)
64. J. Huang, C. Wang, X. Zhang, W. Jia, R. Ma, Z. Yang, T. Dong, Facile preparation and thermal properties of Field's alloy nanofluid for heat transfer. Colloids Surfaces A Physicochem. Eng. Asp. **581**, 123805 (2019)
65. B. Du, Q. Jian, Size controllable synthesis of graphene water nanofluid with enhanced stability. Fullerenes Nanotub. Carbon Nanostructures **27**(1), 87–96 (2019)
66. D. Li, W. Fang, Y. Feng, Q. Geng, M. Song, Stability properties of water-based gold and silver nanofluids stabilized by cationic gemini surfactants. J. Taiwan Inst. Chem. Eng. **97**, 458–465 (2019)
67. I. Wole-Osho, E.C. Okonkwo, D. Kavaz, S. Abbasoglu, An experimental investigation into the effect of particle mixture ratio on specific heat capacity and dynamic viscosity of Al2O3-ZnO hybrid nanofluids. Powder Technol. **363**, 699–716 (2020)
68. X.J. Wang, X. Li, S. Yang, Influence of pH and SDBS on the stability and thermal conductivity of nanofluids. Energy Fuels **23**, 2684–2689 (2009)
69. A. Aureen Albert, D.G. Harris Samuel, V. Parthasarathy, K. Kiruthiga, A facile one pot synthesis of highly stable PVA–CuO hybrid nanofluid for heat transfer application. Chem. Eng. Commun. **207**, 1–12 (2019)

70. H.I. Mohammed, D. Giddings, G.S. Walker, Experimental investigation of nanoparticles concentration, boiler temperature and flow rate on flow boiling of zinc bromide and acetone solution in a rectangular duct. Int. J. Heat Mass Transf. **130**, 710–721 (2019)
71. A.K. Sharma, A.K. Tiwari, A.R. Dixit, Rheological behaviour of nanofluids: a review. Renew. Sustain. Energy Rev. **53**, 779–791 (2016)
72. M.H. Ahmadi, A. Mirlohi, M. Alhuyi Nazari, R. Ghasempour, A review of thermal conductivity of various nanofluids. J. Mol. Liq. **265**, 181–188 (2018)
73. S. Guo, S. Dong, E. Wang, Gold/platinum hybrid nanoparticles supported on multiwalled carbon nanotube/silica coaxial nanocables: Preparation and application as electrocatalysts for oxygen reduction. J. Phys. Chem. C. **112**(7), 2389–93 (2008)
74. B.C. Pak, Y.I. Cho, Hydrodynamic and heat transfer study of dispersed fluids with submicron metallic oxide particles. Exp. Heat Transf. **11**, 151–170 (1998)
75. H. O'Hanley, J. Buongiorno, T. McKrell, L.W. Hu, (2012) Measurement and model validation of nanofluid specific heat capacity with differential scanning calorimetry. Adv. Mech. Eng. **4**, 181079 (2012)
76. Y. Xuan, W. Roetzel, Conceptions for heat transfer correlation of nanofluids. Int. J. Heat Mass Transf. **43**, 3701–3707 (2000)
77. S.M.S. Murshed, Simultaneous measurement of thermal conductivity, thermal diffusivity, and specific heat of nanofluids. Heat Transf. Eng. **33**, 722–731 (2012)
78. L.P. Zhou, B.X. Wang, X.F. Peng, X.Z. Du, Y.P. Yang, On the specific heat capacity of CuO nanofluid. Adv. Mech. Eng. **2**, 172085 (2010)
79. D. Shin, D. Banerjee, Enhancement of specific heat capacity of high-temperature silica-nanofluids synthesized in alkali chloride salt eutectics for solar thermal-energy storage applications. Int. J. Heat Mass Transf. **54**(5–6), 1064–1070 (2011)
80. V. Kumaresan, R. Velraj, Experimental investigation of the thermo-physical properties of water-ethylene glycol mixture based CNT nanofluids. Thermochim. Acta **545**, 180–186 (2012)
81. R.S. Vajjha, D.K. Das, Specific heat measurement of three nanofluids and development of new correlations. J. Heat Transfer. **131**, 7 (2009)
82. I.O. Alade, M.A. Abd Rahman, T.A. Saleh, Predicting the specific heat capacity of alumina/ethylene glycol nanofluids using support vector regression model optimized with Bayesian algorithm. Sol. Energy **183**(2019), 74–82 (2019)
83. M.A. Hassan, D. Banerjee, A soft computing approach for estimating the specific heat capacity of molten salt-based nanofluids. J. Mol. Liq. **281**(2019), 365–375 (2019)
84. M. Saeedinia, M.A. Akhavan-Behabadi, M. Nasr, Experimental study on heat transfer and pressure drop of nanofluid flow in a horizontal coiled wire inserted tube under constant heat flux. Exp. Therm. Fluid Sci. **36**, 158–68 (2012)
85. M.N. Pantzali, A.G. Kanaris, K.D. Antoniadis, A.A. Mouza, S.V. Paras, Effect of nanofluids on the performance of a miniature plate heat exchanger with modulated surface. Int. J. Heat Fluid Flow. **30**, 691–9 (2009)
86. S. Hoseinzadeh, S.A.R. Sahebi, R. Ghasemiasl, A.R. Majidian, Experimental analysis to improving thermosyphon (TPCT) thermal efficiency using nanoparticles/based fluids (water). Eur. Phys. J. Plus **32**(5), 197 (2017)
87. R.L. Hamilton, O.K. Crosser, Thermal conductivity of heterogeneous two-component systems. Ind. Eng. Chem. Fundam. **1**(3), 187–191 (1962)
88. Y. Xuan, Q. Li, *Heat transfer enhancement of nanofluids* (Int. J, Heat Fluid Flow, 2000)
89. W. Yu, S.U.S. Choi, The role of interfacial layers in the enhanced thermal conductivity of nanofluids: a renovated Hamilton-Crosser model. J. Nanoparticle Res. **6**(4), 355–361 (2004)
90. B.X. Wang, L.P. Zhou, X.F. Peng, A fractal model for predicting the effective thermal conductivity of liquid with suspension of nanoparticles. Int. J. Heat Mass Transf. **46**(14), 2665–2672 (2003)
91. B. Yang, Thermal conductivity equations based on brownian motion in suspensions of nanoparticles (nanofluids). J. Heat Transfer. **130**, 4 (2008)
92. Z. Said, M.H. Sajid, M.A. Alim, R. Saidur, N.A. Rahim, Experimental investigation of the thermophysical properties of AL2O3-nanofluid and its effect on a flat plate solar collector. Int. Commun. Heat Mass Transf. **48**, 99–107 (2013)
93. S.M.S. Murshed, K.C. Leong, C. Yang, Enhanced thermal conductivity of TiO2 - Water based nanofluids. Int. J. Therm. Sci. **44**, 367–373 (2005)

94. R. Taherialekouhi, S. Rasouli, A. Khosravi, (2019) An experimental study on stability and thermal conductivity of water-graphene oxide/aluminum oxide nanoparticles as a cooling hybrid nanofluid. Int. J. Heat Mass Transf. **145**, 118751 (2019)
95. I. Wole-Osho, E.C. Okonkwo, H. Adun, D. Kavaz, S. Abbasoglu, An intelligent approach to predicting the effect of nanoparticle mixture ratio, concentration and temperature on thermal conductivity of hybrid nanofluids. J. Therm. Anal. Calorim. **1**, 8 (2020)
96. V.D.A.G. Bruggeman, Berechnung verschiedener physikalischer Konstanten von heterogenen Substanzen. Ann. Phys. **5**, 636–664 (1935)
97. L.E. Nielsen, Generalized equation for the elastic moduli of composite materials. J. Appl. Phys. **41**, 4626–4627 (1970)
98. M. Hemmat Esfe, A. Karimipour, W.M. Yan, M. Akbari, M.R. Safaei, M. Dahari, Experimental study on thermal conductivity of ethylene glycol based nanofluids containing Al2O3 nanoparticles. Int. J. Heat Mass Transf. **88**, 728–734 (2015)
99. M.F. Nabil, W.H. Azmi, K. Abdul Hamid, R. Mamat, F.Y. Hagos, An experimental study on the thermal conductivity and dynamic viscosity of TiO2-SiO2 nanofluids in water: Ethylene glycol mixture. Int. Commun. Heat Mass Transf. **86**, 181–189 (2017)
100. M. Afrand, Experimental study on thermal conductivity of ethylene glycol containing hybrid nano-additives and development of a new correlation. Appl. Therm. Eng. **110**, 1111–1119 (2017)
101. N.N. Esfahani, D. Toghraie, M. Afrand, A new correlation for predicting the thermal conductivity of ZnO–Ag (50%–50%)/water hybrid nanofluid: an experimental study. Powder Technol. **323**, 367–373 (2018)
102. B. Wei, C. Zou, X. Li, Experimental investigation on stability and thermal conductivity of diathermic oil based TiO2 nanofluids. Int. J. Heat Mass Transf. **104**, 537–543 (2017)
103. M. Mehrabi, M. Sharifpur, J.P. Meyer, Application of the FCM-based neuro-fuzzy inference system and genetic algorithm-polynomial neural network approaches to modelling the thermal conductivity of alumina-water nanofluids. Int. Commun. Heat Mass Transf. **39**, 971–977 (2012)
104. M. Hemmat Esfe, W.M. Yan, M. Afrand, M. Sarraf, D. Toghraie, M. Dahari, Estimation of thermal conductivity of Al2O3/water (40%)-ethylene glycol (60%) by artificial neural network and correlation using experimental data. Int. Commun. Heat Mass Transf. **74**, 125–128 (2016)
105. M. Vakili, M. Karami, S. Delfani, S. Khosrojerdi, K. Kalhor, Experimental investigation and modeling of thermal conductivity of CuO–water/EG nanofluid by FFBP-ANN and multiple regressions. J. Therm. Anal. Calorim. **129**, 629–637 (2017)
106. A. Komeilibirjandi, A.H. Raffiee, A. Maleki, M. Alhuyi Nazari, M. Safdari Shadloo, Thermal conductivity prediction of nanofluids containing CuO nanoparticles by using correlation and artificial neural network. J. Therm. Anal. Calorim. **139**(4), 2679–89 (2019)
107. A. Shahsavar, S. Khanmohammadi, D. Toghraie, H. Salihepour, Experimental investigation and develop ANNs by introducing the suitable architectures and training algorithms supported by sensitivity analysis: Measure thermal conductivity and viscosity for liquid paraffin based nanofluid containing Al 2 O 3 nanoparticl. J. Mol. Liq. **279**, 850–860 (2019)
108. A. Khalifeh, B. Vaferi, (2019) Intelligent assessment of effect of aggregation on thermal conductivity of nanofluids—comparison by experimental data and empirical correlations. Thermochim. Acta **681**, 178377 (2019)
109. A. Einstein, Paper 1. A New Determination of Molecular Dimensions (1905)
110. M. Mooney, The viscosity of a concentrated suspension of spherical particles. J. Colloid Sci. **6**(2), 162–170 (1951)
111. D.S. Udawattha, M. Narayana, U.P.L. Wijayarathne, Predicting the effective viscosity of nanofluids based on the rheology of suspensions of solid particles. J. King Saud Univ. - Sci. **31**(3), 412–426 (2017)
112. N. Zhao, X. Wen, J. Yang, S. Li, Z. Wang, Modeling and prediction of viscosity of water-based nanofluids by radial basis function neural networks. Powder Technol. **281**, 173–83 (2015)
113. H. Karimi, F. Yousefi, M.R. Rahimi, Correlation of viscosity in nanofluids using genetic algorithm-neural network (GA-NN). Heat Mass Transf. und Stoffuebertragung. **47**, 1417–25 (2011)
114. I.M. Krieger, T.J. Dougherty, A Mechanism for Non-Newtonian Flow in Suspensions of Rigid Spheres. Trans. Soc. Rheol. **3**, 137–152 (1959)
115. G.K. Batchelor, The effect of Brownian motion on the bulk stress in a suspension of spherical particles. J. Fluid Mech. **83**, 97 (1977)
116. E. Abu-Nada, Effects of variable viscosity and thermal conductivity of Al2O3-water nanofluid on heat transfer enhancement in natural convection. Int. J. Heat Fluid Flow **30**(4), 679–690 (2009)

117. S.M. Hosseini, A.R. Moghadassi, D.E. Henneke, A new dimensionless group model for determining the viscosity of nanofluids. J. Therm. Anal. Calorim. **100**(3), 873–877 (2010)
118. M. Hemmat Esfe, S. Saedodin, An experimental investigation and new correlation of viscosity of ZnO-EG nanofluid at various temperatures and different solid volume fractions. Exp. Therm. Fluid Sci. **55**(2014), 1–5 (2014)
119. W.H. Azmi, K.V. Sharma, R. Mamat, A.B.S. Alias, I. Izwan Misnon, *Correlations for thermal conductivity and viscosity of water based nanofluids* (IOP Conf, Ser. Mater. Sci. Eng., 2012), p. 012029
120. M. Asadi, A. Asadi, Dynamic viscosity of MWCNT/ZnO-engine oil hybrid nanofluid: An experimental investigation and new correlation in different temperatures and solid concentrations. Int. Commun. Heat Mass Transf. **76**(2016), 41–45 (2016)
121. N.N.M. Zawawi, W.H. Azmi, M.Z. Sharif, G. Najafi, Experimental investigation on stability and thermo-physical properties of Al 2 O 3 –SiO 2 /PAG nanolubricants with different nanoparticle ratios. J. Therm. Anal. Calorim. **135**(2), 1243–1255 (2019)
122. M. Sharifpur, S.A. Adio, J.P. Meyer, Experimental investigation and model development for effective viscosity of Al2O3-glycerol nanofluids by using dimensional analysis and GMDH-NN methods. Int. Commun. Heat Mass Transf. **68**(2015), 208–219 (2015)
123. E. Heidari, M.A. Sobati, S. Movahedirad, *Accurate prediction of nanofluid viscosity using a multilayer perceptron artificial neural network (MLP-ANN)* (Chemom. Intell. Lab, Syst, 2016)
124. S.A. Adio, M. Mehrabi, M. Sharifpur, J.P. Meyer, Experimental investigation and model development for effective viscosity of MgO-ethylene glycol nanofluids by using dimensional analysis, FCM-ANFIS and GA-PNN techniques. Int. Commun. Heat Mass Transf. **2016**, 71–83 (2016)
125. M. Hemmat Esfe, M.H. Kamyab, M. Afrand, M.K. Amiri, Using artificial neural network for investigating of concurrent effects of multi-walled carbon nanotubes and alumina nanoparticles on the viscosity of 10W–40 engine oil. Phys. A Stat. Mech. its Appl. **510**(2018), 610–624 (2018)
126. E.V. Timofeeva, A.N. Gavrilov, J.M. McCloskey, Y.V. Tolmachev, S. Sprunt, L.M. Lopatina, J.V. Selinger, Thermal conductivity and particle agglomeration in alumina nanofluids: Experiment and theory. Phys. Rev. E. **76**(6), 061203 (2007)
127. Y. Luo, R. Zhao, J.B. Pendry, van der Waals interactions at the nanoscale: The effects of nonlocality. Proc. Natl. Acad. Sci. **111**(52), 18422–7 (2014)
128. F. London, The general theory of molecular forces. Trans. Faraday Soc. **33**, 8–26 (2004)
129. K.H. Krishna, S. Neti, S. Mohapatra, Modeling of Particle Agglomeration in Nanofluids. J. Appl. Phys. **117**, 094304 (2013)
130. Y. Xuan, Q. Li, P. Tie, The effect of surfactants on heat transfer feature of nanofluids. Exp. Therm. Fluid Sci. **46**, 259–262 (2013)
131. X. Yang, Z. Liu, A kind of nanofluid consisting of surface-functionalized nanoparticles. Nanoscale Res. Lett. **5**, 1324–8 (2010)
132. Y. Hwang, J.K. Lee, C.H. Lee, Y.M. Jung, S.I. Cheong, C.G. Lee, B.C. Ku, S.P. Jang, Stability and thermal conductivity characteristics of nanofluids. Thermochim. Acta. **455**, 70–4 (2007)
133. Z. Said, M.H. Sajid, M.A. Alim, R. Saidur, N.A. Rahim, Experimental investigation of the thermophysical properties of AL 2 O 3 -nano fl uid and its effect on a fl at plate solar collector. Int. Commun. Heat Mass Transf. **48**, 99–107 (2013)
134. C.T. Nguyen, N. Galanis, T. Maré, E. Eveillard, New Viscosity Data for CuO-Water Nanofluid –the Hysteresis Phenomenon Revisited. Adv. Sci. Technol. **81**, 101–106 (2012)
135. M. Faizal, R. Saidur, S. Mekhilef, A. Hepbasli, I.M. Mahbubul, Energy, economic, and environmental analysis of a flat-plate solar collector operated with SiO2 nanofluid. Clean Technol. Environ. Policy **17**, 1457–1473 (2015)
136. S. Salavati Meibodi, A. Kianifar, H. Niazmand, O. Mahian, S. Wongwises, Experimental investigation on the thermal efficiency and performance characteristics of a flat plate solar collector using SiO<inf>2</inf>/EG-water nanofluids. Int. Commun. Heat Mass Transf. **65**, 71–75 (2015)
137. Q. He, S. Zeng, S. Wang, Experimental investigation on the efficiency of flat-plate solar collectors with nanofluids. Appl. Therm. Eng. **88**, 165–171 (2014)
138. S.K. Verma, A.K. Tiwari, D.S. Chauhan, Performance augmentation in flat plate solar collector using MgO / water nanofluid. Energy Convers. Manag. **124**, 607–617 (2016)
139. A.J. Moghadam, M. Farzane-Gord, M. Sajadi, M. Hoseyn-Zadeh, Effects of CuO/water nanofluid on the efficiency of a flat-plate solar collector. Exp. Therm. Fluid Sci. **58**, 9–14 (2014)
140. A. Noghrehabadi, E. Hajidavaloo, M. Moravej, Experimental investigation of efficiency of square flat-plate solar collector using SiO 2 /water nanofluid. Case Stud. Therm. Eng. **8**, 378–386 (2016)

141. S. Salavati Meibodi, A. Kianifar, H. Niazmand, O. Mahian, S. Wongwises, Experimental investigation on the thermal efficiency and performance characteristics of a flat plate solar collector using SiO2/EG-water nanofluids. Int. Commun. Heat Mass Transf. **65**, 71–75 (2015)
142. M.A. Sharafeldin, G. Gróf, Experimental investigation of flat plate solar collector using CeO2-water nanofluid. Energy Convers. Manag. **155**, 32–41 (2018)
143. M.J. Stalin, P., Arjunan, T. V., Matheswaran, M.M., and Sadanandam, N., Experimental and theoretical investigation on the effects of lower concentration CeO 2 /water nanofluid in flat-plate solar collector. J. Therm. Anal. Calorim. **135**, 29–44 (2019)
144. M.A. Sharafeldin, G. Gróf, O. Mahian, Experimental study on the performance of a flat-plate collector using WO3/Water nanofluids. Energy **141**, 2436–2444 (2017)
145. Z. Said, R. Saidur, N.A. Rahim, Energy and exergy analysis of a flat plate solar collector using different sizes of aluminium oxide based nanofluid. J. Clean. Prod. **133**, 518–530 (2016)
146. J.J. Michael, S. Iniyan, Performance of copper oxide/water nanofluid in a flat plate solar water heater under natural and forced circulations. Energy Convers. Manag. **95**, 160–169 (2015)
147. F. Kiliç, T. Menlik, A. Sözen, Effect of titanium dioxide/water nano fl uid use on thermal performance of the fl at plate solar collector. Sol. Energy **164**, 101–108 (2018)
148. T. Yousefi, E. Shojaeizadeh, F. Veysi, S. Zinadini, An experimental investigation on the effect of pH variation of MWCNT-H 2O nanofluid on the efficiency of a flat-plate solar collector. Sol. Energy **86**, 771–779 (2012)
149. D. Lee, J.W. Kim, B.G. Kim, A new parameter to control heat transport in nanofluids: Surface charge state of the particle in suspension. J. Phys. Chem. B. **110**, 4323–8 (2006)
150. E. Shojaeizadeh, F. Veysi, Development of a correlation for parameter controlling using exergy efficiency optimization of an Al2O3/water nanofluid based flat-plate solar collector. Appl. Therm. Eng. **98**, 1116–1129 (2016)
151. Z.P. Yang, L. Ci, J.A. Bur, S.Y. Lin, P.M. Ajayan, Experimental observation of an extremely dark material made by a low-density nanotube array. Nano Lett. **8**, 446–51 (2008)
152. Z. Said, R. Saidur, M.A. Sabiha, N.A. Rahim, M.R. Anisur, Thermophysical properties of Single Wall Carbon Nanotubes and its effect on exergy efficiency of a flat plate solar collector. Sol. Energy **115**, 757–769 (2015)
153. A. Ahmadi, D.D. Ganji, F. Jafarkazemi, Analysis of utilizing Graphene nanoplatelets to enhance thermal performance of flat plate solar collectors. Energy Convers. Manag. **126**, 1–11 (2016)
154. Z. Said, M.A. Alim, I. Janajreh, Exergy efficiency analysis of a flat plate solar collector using graphene based nanofluid. IOP Conf. Ser. Mater. Sci. Eng. **92**, 1 (2015)
155. S.K. Verma, A.K. Tiwari, D.S. Chauhan, Experimental evaluation of flat plate solar collector using nanofluids. Energy Convers. Manag. **134**, 103–115 (2017)
156. S.K. Verma, A.K. Tiwari, S. Tiwari, D.S. Chauhan, Performance analysis of hybrid nanofluids in flat plate solar collector as an advanced working fluid. Sol. Energy **167**, 231–241 (2018)
157. K.A. Hamid, W.H. Azmi, M.F. Nabil, R. Mamat, K.V. Sharma, Experimental investigation of thermal conductivity and dynamic viscosity on nanoparticle mixture ratios of TiO2-SiO2 nanofluids. Int. J. Heat Mass Transf. **116**, 1143–1152 (2018)
158. F.R. Siddiqui, C.Y. Tso, K.C. Chan, S.C. Fu, C.Y.H. Chao, On trade-off for dispersion stability and thermal transport of Cu-Al2O3 hybrid nanofluid for various mixing ratios. Int. J. Heat Mass Transf. **132**, 1200–1216 (2019)
159. M. Mirzaei, Experimental investigation of CuO nanofluid in the thermal characteristics of a flat plate solar collector. Environ. Prog. Sustain. Energy **38**, 260–267 (2019)
160. Z. Said, R. Saidur, N.A. Rahim, M.A. Alim, Analyses of exergy efficiency and pumping power for a conventional flat plate solar collector using SWCNTs based nanofluid. Energy Build. **78**, 1–9 (2014)
161. T. Yousefi, F. Veisy, E. Shojaeizadeh, S. Zinadini, An experimental investigation on the effect of MWCNT-H2O nanofluid on the efficiency of flat-plate solar collectors. Exp. Therm. Fluid Sci. **39**, 207–12 (2012)
162. G.A. Pise, S.S. Salve, A.T. Pise, A.A. Pise, Investigation of solar heat pipe collector using nanofluid and surfactant. Energy Procedia **90**, 481–491 (2015)
163. H. Kim, J. Kim, H. Cho, Experimental study on performance improvement of U-tube solar collector depending on nanoparticle size and concentration of Al2O3 nanofluid. Energy **118**, 1304–1312 (2017)

164. J. Ghaderian, N.A.C. Sidik, An experimental investigation on the effect of Al 2 O 3 /distilled water nanofluid on the energy efficiency of evacuated tube solar collector. Int. J. Heat Mass Transf. **108**, 972–987 (2017)
165. A.A. Eidan, A. AlSahlani, A.Q. Ahmed, M. Al-fahham, J.M. Jalil, Improving the performance of heat pipe-evacuated tube solar collector experimentally by using Al2O3 and CuO/acetone nanofluids. Sol. Energy **173**, 780–788 (2018)
166. B. Jiao, L.M. Qiu, X.B. Zhang, Y. Zhang, Investigation on the effect of filling ratio on the steady-state heat transfer performance of a vertical two-phase closed thermosyphon. Appl. Therm. Eng. **36**, 22–9 (2008)
167. Y.Y. Gan, H.C. Ong, T.C. Ling, N.W.M. Zulkifli, C.T. Wang, Y.C. Yang, Thermal conductivity optimization and entropy generation analysis of titanium dioxide nanofluid in evacuated tube solar collector. Appl. Therm. Eng. **145**, 155–164 (2018)
168. Z. Mingzheng, X. Guodong, L. Jian, C. Lei, Z. Lijun, Analysis of factors influencing thermal conductivity and viscosity in different kinds of surfactant solutions. Exp. Therm. Fluid Sci. **36**, 22–9 (2012)
169. M. Mahendran, T.Z.S. Ali, A. Shahrani, R.A. Bakar, The Efficiency Enhancement on the Direct Flow Evacuated Tube Solar Collector Using Water-Based Titanium Oxide Nanofluids. Appl. Mech. Mater. **465–466**, 308–315 (2013)
170. M.A. Sharafeldin, G. Gróf, Evacuated tube solar collector performance using CeO2/water nanofluid. J. Clean. Prod. **185**, 347–356 (2018)
171. M.A. Sharafeldin, G. Gróf, Efficiency of evacuated tube solar collector using WO 3 /Water nanofluid. Renew. Energy **134**, 453–460 (2019)
172. H. Kaya, K. Arslan, N. Eltugral, Experimental investigation of thermal performance of an evacuated U-Tube solar collector with ZnO/Etylene glycol-pure water nanofluids. Renew. Energy **122**, 329–338 (2018)
173. S. Yan, F. Wang, Z.G. Shi, R. Tian, Heat transfer property of SiO2/water nanofluid flow inside solar collector vacuum tubes. Appl. Therm. Eng. **118**, 385–391 (2017)
174. A. Ozsoy, V. Corumlu, Thermal performance of a thermosyphon heat pipe evacuated tube solar collector using silver-water nanofluid for commercial applications. Renew. Energy **122**, 26–34 (2018)
175. E. Bulut, M. Özacar, Rapid, facile synthesis of silver nanostructure using hydrolyzable tannin. Ind. Eng. Chem. Res. **48**, 5686–5690 (2009)
176. A.H. Hussain, Q. Jawad, K.F. Sultan, Experimental analysis on thermal efficiency of evacuated tube solar collector by using nanofluids. Int. J. Sustain. Green Energy **4**, 19–28 (2015)
177. I.M. Mahbubul, M.M.A. Khan, N.I. Ibrahim, H.M. Ali, F.A. Al-Sulaiman, R. Saidur, Carbon nanotube nanofluid in enhancing the efficiency of evacuated tube solar collector. Renew. Energy **121**, 36–44 (2018)
178. S. Iranmanesh, H.C. Ong, B.C. Ang, E. Sadeghinezhad, A. Esmaeilzadeh, M. Mehrali, Thermal performance enhancement of an evacuated tube solar collector using graphene nanoplatelets nanofluid. J. Clean. Prod. **162**, 121–129 (2017)
179. H. Kim, J. Ham, C. Park, H. Cho, Theoretical investigation of the efficiency of a U-tube solar collector using various nanofluids. Energy **94**, 497–507 (2016)
180. L. Lu, Z.H. Liu, H.S. Xiao, Thermal performance of an open thermosyphon using nanofluids for high-temperature evacuated tubular solar collectors Part 1: Indoor experiment. Sol. Energy **85**, 379–387 (2011)
181. Z.H. Liu, R.L. Hu, L. Lu, F. Zhao, H.S. Xiao, Thermal performance of an open thermosyphon using nanofluid for evacuated tubular high temperature air solar collector. Energy Convers. Manag. **73**, 135–143 (2013)
182. H. Olia, M. Torabi, M. Bahiraei, M.H. Ahmadi, M. Goodarzi, M.R. Safaei, Application of nanofluids in thermal performance enhancement of parabolic trough solar collector: state-of-the-art. Appl. Sci. **9**(3), 463 (2019)
183. S.E. Ghasemi, A.A. Ranjbar, Thermal performance analysis of solar parabolic trough collector using nano fl uid as working fl uid : A CFD modelling study. J. Mol. Liq. **222**, 159–166 (2016)
184. J. Subramani, P.K. Nagarajan, O. Mahian, R. Sathyamurthy, Efficiency and heat transfer improvements in a parabolic trough solar collector using TiO2 nanofluids under turbulent flow regime. Renew. Energy **119**, 19–31 (2018)
185. M. Potenza, M. Milanese, G. Colangelo, A. de Risi, Experimental investigation of transparent parabolic trough collector based on gas-phase nanofluid. Appl. Energy **203**, 560–570 (2017)

186. G. Coccia, G. Di Nicola, L. Colla, L. Fedele, M. Scattolini, Adoption of nanofluids in low-enthalpy parabolic trough solar collectors: Numerical simulation of the yearly yield. Energy Convers. Manag. **118**, 306–319 (2016)
187. E.C. Okonkwo, E.A. Essien, E. Akhayere, M. Abid, D. Kavaz, T.A.H. Ratlamwala, Thermal performance analysis of a parabolic trough collector using water-based green-synthesized nanofluids. Sol. Energy **170**, 658–670 (2018)
188. E.C. Okonkwo, M. Abid, T.A.H. Ratlamwala, S. Abbasoglu, M. Dagbasi, Optimal analysis of entropy generation and heat transfer in parabolic trough collector using green-synthesized TiO2/water nanofluids. J. Sol. Energy Eng. **141**, 3 (2018)
189. A. Mwesigye, Z. Huan, J.P. Meyer, Thermal performance and entropy generation analysis of a high concentration ratio parabolic trough solar collector with Cu-Therminol®VP-1 nanofluid. Energy Convers. Manag. **120**, 449–465 (2016)
190. E.C. Okonkwo, M. Abid, T.A.H. Ratlamwala, Numerical analysis of heat transfer enhancement in a parabolic trough collector based on geometry modifications and working fluid usage. J. Sol. Energy Eng. **1**, 40 (2018)
191. E.C. Okonkwo, E.A. Essien, D. Kavaz, M. Abid, T.A.H. Ratlamwala, Olive leaf synthesized nanofluids for solar parabolic trough collector-thermal performance evaluation. J. Therm. Sci. Eng. Appl. **14**, 4 (2019)
192. Y. Wang, J. Xu, Q. Liu, Y. Chen, H. Liu, Performance analysis of a parabolic trough solar collector using Al2O3/synthetic oil nanofluid. Appl. Therm. Eng. **107**, 469–478 (2016)
193. E. Bellos, C. Tzivanidis, (2017) Parametric investigation of nanofluids in parabolic trough collectors. Therm. Sci. Eng. Prog. **2**(127), 736–747 (2017)
194. T. Sokhansefat, A.B. Kasaeian, F. Kowsary, Heat transfer enhancement in parabolic trough collector tube using Al2O3/synthetic oil nanofluid. Renew. Sustain. Energy Rev. **33**, 636–644 (2014)
195. A. Mwesigye, Z. Huan, J.P. Meyer, Thermodynamic optimisation of the performance of a parabolic trough receiver using synthetic oil–Al2O3 nanofluid. Appl. Energy **156**, 398–412 (2015)
196. E. Bellos, C. Tzivanidis, Thermal analysis of parabolic trough collector operating with mono and hybrid nanofluids. Sustain. Energy Technol. Assessments **26**, 105–115 (2018)
197. A.A. Minea, Hybrid nanofluids based on Al2O3, TiO2and SiO2: numerical evaluation of different approaches. Int. J. Heat Mass Transf. **104**, 852–860 (2017)
198. A.A. Minea, W.M. El-Maghlany, Influence of hybrid nanofluids on the performance of parabolic trough collectors in solar thermal systems: recent findings and numerical comparison. Renew. Energy **120**, 350–364 (2018)
199. K. Sunil, L.A.L. Kundan, S. Sumeet, Performance Evaluation of a Nanofluid Based Parabolic Solar Collector – an Experimental Study. *Proc. Twelveth IRF Int. Conf. 31st August 2014, Chennai, India, ISBN 978–93–84209–48–3*, (August), 29–35 (2014)
200. F.R. Bilal, U.C. Arunachala, H.M. Sandeep, *Experimental validation of energy parameters in parabolic trough collector with plain absorber and analysis of heat transfer enhancement techniques* (J. Phys. Conf, Ser, 2018)
201. M. Hatami, J. Geng, D. Jing, Enhanced efficiency in Concentrated Parabolic Solar Collector (CPSC) with a porous absorber tube filled with metal nanoparticle suspension. Green Energy Environ. **3**, 129–37 (2018)
202. A. Mwesigye, İ.H. Yılmaz, J.P. Meyer, Numerical analysis of the thermal and thermodynamic performance of a parabolic trough solar collector using SWCNTs-Therminol®VP-1 nanofluid. Renew. Energy. **119**, 844–62 (2018)
203. E.C. Okonkwo, M. Abid, T.A.H. Ratlamwala, Effects of synthetic oil nanofluids and absorber geometries on the exergetic performance of the parabolic trough collector. Int. J. energy Res. **42**, 3559–3574 (2018)
204. J. Subramani, P.K. Nagarajan, S. Wongwises, S.A. El-Agouz, R. Sathyamurthy, Experimental study on the thermal performance and heat transfer characteristics of solar parabolic trough collector using Al2O3 nanofluids. Environ. Prog. Sustain. Energy **37**, 1149–1159 (2018)
205. A. Kasaeian, S. Daviran, R.D. Azarian, A. Rashidi, Performance evaluation and nanofluid using capability study of a solar parabolic trough collector. Energy Convers. Manag. **89**, 368–75 (2015)
206. A. Menbari, A.A. Alemrajabi, A. Rezaei, Heat transfer analysis and the effect of CuO/Water nanofluid on direct absorption concentrating solar collector. Appl. Therm. Eng. **104**, 176–83 (2016)
207. K. Chaudhari, P. Walke, U. Wankhede, R. Shelke, An Experimental Investigation of a Nanofluid (Al2O3+H2O) based parabolic trough solar collectors. Br. J. Appl. Sci. Technol. **5**, 551–7 (2015)

208. N. Basbous, M. Taqi, N. Belouaggadia, C. Author, Numerical study of a parabolic trough collector using a nanofluid. Asian J. Curr. Eng. Maths. **4**, 40–44 (2015)
209. E. Bellos, C. Tzivanidis, K.A. Antonopoulos, G. Gkinis, Thermal enhancement of solar parabolic trough collectors by using nanofluids and converging-diverging absorber tube. Renew. Energy **94**, 213–222 (2016)
210. E. Kaloudis, E. Papanicolaou, V. Belessiotis, Numerical simulations of a parabolic trough solar collector with nanofluid using a two-phase model. Renew. Energy, 97: 29 (2016)
211. A. Mwesigye, Z. Huan, Thermodynamic analysis and optimization of fully developed turbulent forced convection in a circular tube with water-Al2O3 nanofluid Int. J. Heat Mass Transf. **89**, 706 (2015)
212. A. Kasaeian, R. Daneshazarian, R. Rezaei, F. Pourfayaz, G. Kasaeian, Experimental investigation on the thermal behavior of nanofluid direct absorption in a trough collector. J. Clean. Prod. **158**, 276–284 (2017)
213. V. Khullar, H. Tyagi, P.E. Phelan, T.P. Otanicar, H. Singh, R.A. Taylor, Solar Energy Harvesting Using Nanofluids-Based Concentrating Solar Collector. *ASME 2012 Third Int. Conf. Micro/Nanoscale Heat Mass Transf* (2012)
214. Y.K. Nayak, S.P. Sharma, U.K. Sinha, P. Kumar, N. Kumar, A Novel Solution Methodology for the Optimization of Thermal Analysis in the Solar Parabolic Trough Collector. Indian J. Sci. Technol **9**, 48 (2016)
215. A. Allouhi, M. Benzakour Amine, R. Saidur, T. Kousksou, A. Jamil, Energy and exergy analyses of a parabolic trough collector operated with nanofluids for medium and high temperature applications. Energy Convers. Manag. **155**, 201–17 (2018)
216. W.J. Gerken, A.V. Thomas, N. Koratkar, M.A. Oehlschlaeger, Nanofluid pendant droplet evaporation: experiments and modeling. Int. J. Heat Mass Transf. **74**, 263–8 (2014)
217. C.T. Nguyen, F. Desgranges, G. Roy, N. Galanis, T. Maré, S. Boucher, H. Mintsa, Temperature and particle-size dependent viscosity data for water-based nanofluids - Hysteresis phenomenon. Int. J. Heat Fluid Flow. **28**(6), 1492–1506 (2007)
218. M. Shahul Hameed, S. Suresh, R.K. Singh, Comparative study of heat transfer and friction characteristics of water-based Alumina–copper and Alumina–CNT hybrid nanofluids in laminar flow through pipes. J. Therm. Anal. Calorim. **136**, 243–253 (2019)
219. Y. Xuan, Q. Li, Investigation on convective heat transfer and flow features of nanofluids. J. Heat Transfer **125**, 151 (2003)
220. H.D. Koca, S. Doganay, A. Turgut, I.H. Tavman, R. Saidur, I.M. Mahbubul, Effect of particle size on the viscosity of nanofluids: a review Renew. Sustain. Energy Rev. **82**(1664), 74 (2018)
221. H. Chen, Y. Ding, Y. He, C. Tan, Rheological behaviour of ethylene glycol based titania nanofluids. Chem. Phys. Lett. **444**, 333–337 (2007)
222. Y. Feng, B. Yu, P. Xu, M. Zou, The effective thermal conductivity of nanofluids based on the nanolayer and the aggregation of nanoparticles. J. Phys. D. Appl. Phys. **40**, 3164 (2007)